

# **GEOPHYSICAL SIGNALS OF FAULTS AND LINEAMENTS**

**Author: Kiana Rezaei Asa**

Master's thesis in Petroleum Geoscience - Geophysics

Supervisor: Karl Fabian

Co-supervisor: Tim Redfield

September 2023

Norwegian University of Science and Technology

Faculty of Engineering

Department of Geoscience and Petroleum



## ABSTRACT

This research aims to investigate the effectiveness of geomagnetic methods for identifying geological faults and to understand how faults impact magnetic field diagrams. Additionally, the study explores the underlying reasons for magnetic anomalies observed in fault zones. The primary lithologies in the study area are sandstone and claystone, which can contain iron-bearing minerals that influence magnetic properties under faulting processes. By addressing these objectives, the research seeks to determine whether geomagnetic surveys can reliably detect faults, how faults alter magnetic field patterns, and the specific faulting processes responsible for these magnetic anomalies. The findings are expected to enhance fault detection techniques, improve the interpretation of magnetic data, and provide deeper insights into the dynamics of fault zones.



## SAMMENDRAG

Denne forskningen har som mål å undersøke effektiviteten av geomagnetiske metoder for å identifisere geologiske forkastninger og forstå hvordan forkastninger påvirker magnetiske feltdiagrammer. I tillegg utforsker studien de underliggende årsakene til magnetiske anomalier observert i forkastningssoner. De primære litologiene i studieområdet er sandstein og leirstein, som kan inneholde jernholdige mineraler som påvirker magnetiske egenskaper under forkastningsprosesser. Ved å adressere disse målene søker forskningen å fastslå om geomagnetiske undersøkelser pålitelig kan oppdage forkastninger, hvordan forkastninger endrer magnetiske feltmønstre, og de spesifikke forkastningsprosessene som er ansvarlige for disse magnetiske anomaliene. Funnene er forventet å forbedre teknikker for forkastningsdeteksjon, forbedre tolkningen av magnetiske data, og gi dypere innsikt i dynamikken til forkastningssoner.



## PREFACE

This thesis explores the intriguing study of magnetic anomalies in fault zones, a crucial yet complex area of geophysics and geological surveys. The primary goal of this research is to enhance geomagnetic methods for fault identification, while also investigating how faults influence magnetic field patterns and the reasons behind these changes. My fascination with this topic arises from the intricate geological processes that alter magnetic properties, and the potential to reveal significant insights about subsurface structures through magnetic surveys.

Completing this thesis involved extensive fieldwork, detailed data analysis, and comprehensive theoretical research. Throughout this journey, I have received immense support and encouragement from several individuals, to whom I am deeply grateful.

First and foremost, I would like to thank my mom, Faranak, and my husband, Milad, for their unwavering support and belief in me. Their constant encouragement has been a vital source of motivation.

I am profoundly grateful to my supervisor, Professor Karl Fabian, for his expert guidance and invaluable advice that have greatly influenced this research. I also wish to thank Nathan Church for his assistance during my project. Additionally, my appreciation goes to the faculty and staff of the Department of Geoscience and Petroleum at NTNU, whose resources and support were essential for this study.

Through this research, I aim to contribute to the understanding of fault zone dynamics and improve the interpretation of magnetic anomalies, thereby advancing the broader field of geophysics and geological exploration. I hope the insights and findings presented in this thesis will inspire further research and innovation in the study of magnetic properties of fault rocks.



# CONTENTS

<b>Abstract</b>	<b>i</b>
<b>SAMMENDRAG</b>	<b>ii</b>
<b>Preface</b>	<b>iii</b>
<b>Contents</b>	<b>v</b>
<b>List of Figures</b>	<b>v</b>
<b>1 Introduction</b>	<b>1</b>
1.1 Why it is Important to Identify Faults in Petroleum Systems? . . . . .	1
1.1.1 Overview of the Article: The Role of faults in Hydrocarbon Migration . . . . .	6
1.2 Purpose of this Study . . . . .	7
<b>2 Theory</b>	<b>9</b>
2.1 Understanding Faulting Processes Through Magnetic Properties of Fault Rocks . . . . .	9
2.2 Geomagnetic Method to Identify Faults and Lineaments . . . . .	11
2.2.1 Methods for Identifying and Analyzing Magnetic Anomalies and their Sources . . . . .	12
2.3 Other Geophysical Methods for Identifying Faults and Fractures . . . . .	14
2.3.1 Seismic Surveying Overview . . . . .	14
2.3.2 Geoelectric Data . . . . .	16
2.4 Høybakken Area: Geological and Tectonic Overview . . . . .	17
<b>3 Methods</b>	<b>21</b>
3.1 Research Objective and Hypotheses . . . . .	21
3.1.1 Hypotheses . . . . .	21
3.2 Magnetic Surveying Equipment . . . . .	22
3.2.1 Description of Magnetometer . . . . .	22
3.3 Selection of Study Area . . . . .	24
3.3.1 Placement of Survey Transects . . . . .	26
3.4 Data Collection . . . . .	27
3.4.1 Magnetic Field Measurements . . . . .	27
3.4.2 Quality Control and Data Preprocessing . . . . .	28

3.4.3	Data Calibration	29
3.5	Data Processing	29
3.5.1	Correction, Smoothing, and Plotting Magnetic Field Data Over Time	29
3.5.2	Plotting GPS Data and Visualizing Magnetic Field Variations Over Geographic Coordinates	33
3.5.3	Geospatial Visualization of Magnetic Field Intensity	36
3.5.4	Comparative Analysis of Magnetic Field Data Across Multiple Survey Passes	40
3.5.5	Correlation of Magnetic Field Anomalies with Geological Features	42
3.5.6	Summary of Methodology	46
3.5.7	Relevance to Research Objectives	48
<b>4</b>	<b>Results and conclusion</b>	<b>51</b>
4.1	Future Work Suggestions	52
<b>Appendices:</b>		<b>55</b>
.1	Python Codes	55

## LIST OF FIGURES

1.1.1 structural traps connected to petroleum reservoirs. In both scenarios, rocks with low porosity and permeability cover reservoir rocks with higher porosity and permeability. In both situations, the flaw acts as a sealing flaw, permitting the storage of oil and gas.[3]	3
2.4.1 Geological map of the Høybakken area, detailing the distribution of geological units and structural features. This map highlights the location of the Høybakken detachment fault and its interactions with surrounding rock units and fault systems [12].	17
2.4.2 Schematic block diagram showing relationships between structural elements observed in the hanging wall of the Høybakken detachment fault in the Høybakken-Austrått area. This diagram illustrates the interaction between the Høybakken detachment fault and NE-SW trending faults of the Møre-Trøndelag Fault Complex.[12]	18
3.2.1 G-859AP Mining Magnetometer	22
3.3.1 Geological map showing the locations of Dataset 1, Dataset 2, and Dataset 3 within the Høybakken area. Dataset 1 is located near Hegvik, close to the coast, characterized by meta-igneous rocks and sedimentary deposits. Dataset 2 is positioned within the transition zone between the footwall and hanging wall of the Høybakken detachment fault, notable for its banded cataclasites and ultracataclasites. Dataset 3 is situated near the intersection of the Høybakken detachment fault with the Møre-Trøndelag Fault Complex, an area marked by complex fault interactions and diverse lithologies. [14]	25
3.4.1 Observation of rock's magnetic field on both sides of the fault	28
3.5.1 Smoothed Corrected Magnetic Field Over Time. This plot illustrates the variations in the magnetic field strength, measured in nanoTesla (nT), against time in seconds, ranging from 54,000 to 59,000 seconds. Notable features include sharp declines and subsequent recoveries in magnetic field values, suggesting potential geological anomalies. The smoothing of data highlights significant trends while minimizing the impact of high-frequency noise, aiding in the identification of patterns potentially related to underlying geological structures.	31

3.5.2 This plot represents the variations in the magnetic field strength, measured in nanoTesla (nT), against time in seconds, ranging from 54,000 to 61,200 seconds. The data displayed has been smoothed and corrected to minimize the influence of noise and non-local magnetic fields, emphasizing significant trends and anomalies. . . . .	32
3.5.3 This plot depicts the variations in the magnetic field strength, measured in nanoTesla (nT), against time in seconds, ranging from 53,200 to 57,200 seconds. The magnetic field data has been smoothed and corrected to emphasize significant changes and highlight the overall trends over the observed period. . . . .	32
3.5.4 Latitude, Longitude, and Altitude Variation Over Time in Dataset1. This set of three graphs tracks the changes in latitude, longitude, and altitude over time, measured in seconds. The continuous lines represent the paths and elevation changes recorded during data collection, highlighting geographic movements and altitude variations that may influence magnetic field measurements. . . . .	34
3.5.5 This set of three graphs from dataset2 displays the changes in latitude (top graph), longitude (middle graph), and altitude (bottom graph) over time, measured in seconds from 66,000 to 61,200. These graphs collectively represent the GPS tracking data of a moving object, providing insights into its trajectory and changes in elevation over time. . . . .	35
3.5.6 This series of graphs from dataset3 illustrates the changes in GPS coordinates and altitude from time 62,000 to 67,000 seconds. These combined variations help to trace the path and terrain navigated by the subject during the observation period. . . . .	36
3.5.7 Dataset1 . . . . .	37
3.5.8 Dataset2 . . . . .	37
3.5.9 Dataset3 . . . . .	37
3.5.10 3D plots of corrected magnetic field variation over GPS coordinates for three different datasets. . . . .	37
3.5.11 Dataset1 . . . . .	38
3.5.12 Dataset2 . . . . .	38
3.5.13 Dataset3 . . . . .	38
3.5.14 2D plots of corrected magnetic field variation over GPS coordinates for three different datasets. . . . .	38
3.5.15 This figure displays the $\Delta F$ (measured in nanoteslas, nT) along a predefined path on a geographical map (Dataset1). The color gradient represents different intensities of the magnetic field anomalies, ranging from -200 nT to -340 nT. . . . .	39
3.5.16 This map illustrates the spatial $\Delta F$ recorded during the second geomagnetic survey(Dataset2). The color gradient represents $\Delta F$ measured in nanoteslas (nT), ranging from -180 nT to -210 nT across the surveyed path. . . . .	40
3.5.17 This figure displays the $\Delta F$ measured in nanoteslas (nT) along a survey path during a specific interval (Dataset3). The color gradient from green to purple represents $\Delta F$ ranging from -40 nT to -200 nT. . . . .	41
3.5.18 $\Delta F$ during the First Survey (56700s to 57000s) . . . . .	41
3.5.19 $\Delta F$ during the Second Survey (57000s to 57400s) . . . . .	41

3.5.20	Comparative Visualization of $\Delta F$ during Two Survey Passes. These maps show-case the magnetic field measurements taken during consecutive surveys along the same route, illustrated side by side to highlight the reproducibility of data and detect any significant variations or anomalies. The consistent color scheme across both maps allows for a direct comparison, enhancing the evaluation of temporal stability and geological influences on the magnetic field. . . . .	41
3.5.21	Integrated Geological and $\Delta F$ across a Fault Line.Dataset1. Geological Map From NGU.[14] . . . . .	43
3.5.22	Integrated Geological and $\Delta F$ Data across a Fault Line.Dataset2. Geological Map From NGU.[14] . . . . .	44
3.5.23	Integrated Geological and $\Delta F$ Data across a Fault Line.Dataset3. Geological Map From NGU.[14] . . . . .	46



---

# CHAPTER **ONE**

---

## INTRODUCTION

Exploring the subsurface structure is very interesting to me because of its crucial importance in the petroleum industry. Understanding faults and fractures is critical for a petroleum geophysicist since they have a significant impact on oil and gas systems, influencing everything from exploration to production. Faults and fractures have a substantial impact on hydrocarbon migration, trapping, and reservoir categorization, therefore precise identification is critical for successful exploration and efficient production.

Geophysical methods are often used to locate subsurface elements. However, the focus on geomagnetic approaches has been limited thus far. Geomagnetic technologies have various features that make them ideal for subsurface investigation. They are less expensive than other geophysical techniques and available at all times, making them an affordable and accessible tool for continuous monitoring and data collecting. These approaches also have the advantage of being non-invasive, reducing environmental impact and operating disturbance.

### 1.1 Why it is Important to Identify Faults in Petroleum Systems?

Faults play a crucial role in petroleum systems, influencing the formation, migration, trapping, and production of hydrocarbons (oil and gas). Successful exploration and production operations in the oil and gas sector depend on an understanding of faults. In petroleum systems, defects are significant for the following main reasons:

- **Hydrocarbon Migration:** In hydrocarbon exploration, oil and gas migrate due to buoyant force<sup>1</sup>, as they are less dense than formation water. Highly permeable rocks facilitate migration because of their hydromechanical properties, low capillary pressure<sup>2</sup>, and high permeability, while shaly

---

<sup>1</sup>The upward force exerted on an object submerged in a fluid (in this context, hydrocarbons in formation water) due to the difference in density between the object and the fluid.

<sup>2</sup>In fluid statics, capillary pressure is the pressure between two immiscible fluids in a thin tube, resulting from the interactions of forces between the fluids and solid walls of the tube. Capillary pressure can serve as both an opposing or driving force for fluid transport and is

and evaporitic rocks act as barriers and seals, impeding the migration process.

One of the critical aspects in the oil and gas system where the presence and detection of faults are important is the migration of hydrocarbons. In a non-faulted basin, drainages contain sandstones known as bearing beds, which also act as reservoirs. However, in the presence of faults, the conditions can be different. Faults can act as migration paths or barriers. For example, in extensional areas such as the Gulf of Mexico, oil spills are mainly along salt-related faults, while in complex compressive areas such as the sub-Andean region of Bolivia, a significant percentage of oil and gas leaks are found in faults.[1]

Factors such as displacement, lithology of rocks, types of faults, microcracks, and hydromechanical characteristics<sup>3</sup> of faults can affect the permeability and porosity of the reservoir. In summary, faults play an important role in the migration of hydrocarbons in the Earth's crust. Their permeability characteristics, complexities, and evolution significantly affect fluid flow and influence the overall migration balance in a basin.[1]

- **Fault as a Trap:** Faults can act as traps in hydrocarbon reservoirs by creating structural configurations that prevent the migration of hydrocarbons, effectively accumulating them in specific locations.[2] Mechanism of faults acting as traps:
  - **Fault Structural Traps (FSTs):** Fault structural traps are specific geological formations where faults intersect or interact with rock layers to create a sealed environment that can trap hydrocarbons. These traps are formed by the displacement of rock layers along fault lines. This displacement can juxtapose permeable reservoir rocks against impermeable cap rocks or other barriers, creating a sealed compartment.[2]
  - **Fault Connectivity and Sealing:** For a fault to act as a trap, it must have sealing properties. This means that the fault or the material within the fault zone must be impermeable to hydrocarbons. Various factors, such as clay smearing, mineral precipitation, or fault gouge, can contribute to the sealing properties of a fault. When faults are connected in a way that forms a closed loop or compartment, they can effectively trap hydrocarbons.[2]
  - **Trap Formation Conditions:** Fault structural traps are often associated with the up-dip direction of a reservoir. This means that hydrocarbons migrate up the slope of the reservoir rock until they encounter a fault that prevents further migration. These closed structures are potential traps where hydrocarbons can accumulate.[2]
- **Reservoir compartmentalization:** Reservoir compartmentalization is the partition of a reservoir into separate portions, each having its own fluid flow

---

a significant property for research and industrial purposes (namely microfluidic design and oil extraction from porous rock). It is also observed in natural phenomena.

<sup>3</sup>Pertaining to the mechanical behavior of fluids in porous rocks, considering factors like permeability.

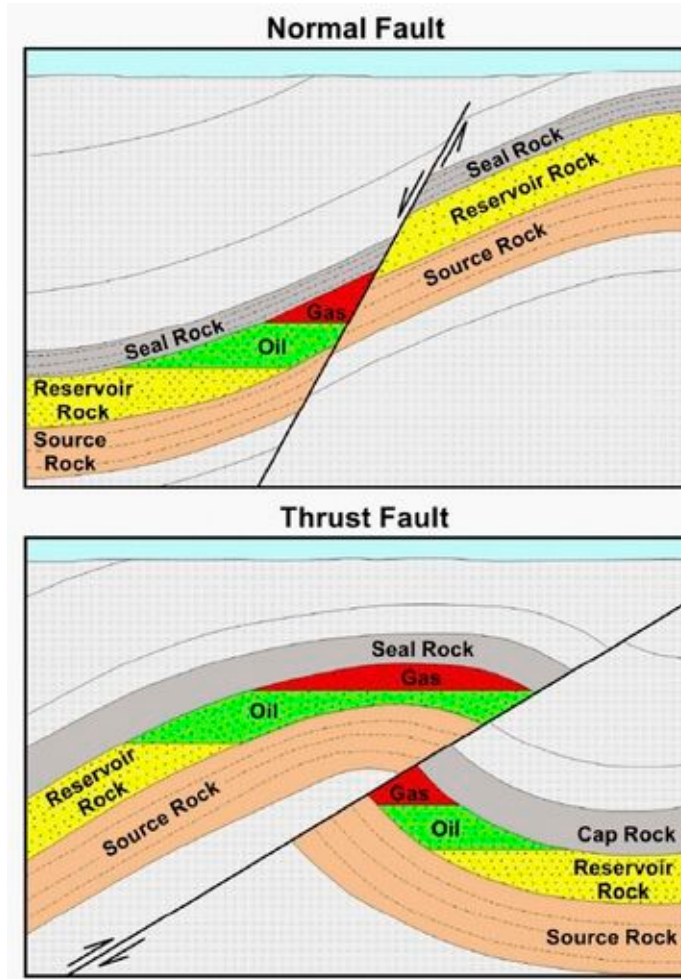


**Figure 1.1.1:** structural traps connected to petroleum reservoirs. In both scenarios, rocks with low porosity and permeability cover reservoir rocks with higher porosity and permeability. In both situations, the flaw acts as a sealing flaw, permitting the storage of oil and gas.[3]

and pressure behavior. Faults can operate as barriers, isolating areas of the reservoir and forming distinct compartments. Identifying these faults aids in determining the distribution and retention of hydrocarbons, as well as understanding the reservoir's potential and constraints.[4]

Faults are important components of reservoir models because they impact the reservoir's three-dimensional shape and thus fluid flow behavior. Understanding the fault network enables historical matching, production scenario predictions, and informed field development decisions. [4]

Faults can operate as conduits for fluid leakage or migration between reservoirs, compromising well integrity<sup>4</sup> and contaminating nearby formations. Understanding fault behavior enables operators to evaluate and minimize these risks during exploration, drilling, and production activities, ultimately enhancing the safety and environmental performance of oil operations.[4]

Operators can make more educated decisions about well placement, development methods, and reservoir management by accurately describing faults and understanding their impact on fluid flow behavior. Effective compartmentalization management can increase hydrocarbon recovery, reservoir performance, and, ultimately, project economics.[4]

To summarize, finding faults and understanding their function in reservoir compartmentalization is critical for optimizing hydrocarbon output, understanding reservoir behavior, and making economically sound decisions in the petroleum sector. Accurate fault characterisation improves reservoir modeling accuracy and helps control the risks associated with fault behavior, resulting in effective exploration, development, and production operations.

- **Fractured Reservoirs:** Faults are significant geological features that often form due to tectonic forces. These forces cause stress in the Earth's crust, leading to the creation of fractures. The process of faulting generates fractures, which can vary in size and connectivity. In naturally fractured carbonate reservoirs, faults frequently create high-permeability zones. These faults are connected to numerous fractures with varying conductivities, enhancing the overall permeability of the reservoir. Faults in fractured reservoirs play a crucial role by establishing connectivity and hydraulic communication, significantly impacting reservoir modeling, and influencing pressure transient behavior:[2]
  - Faults and fractures in naturally fractured reservoirs (NFRs) can either form discrete networks or continuous conductive networks. In some cases, faults create a network of fractures that communicate hydraulically, providing overall conductivity and permeability to the reservoir. The connectivity established by faults and fractures determines the flow paths for hydrocarbons. Faults can act as conduits that facilitate the migration of oil and gas, directing them towards traps where they accumulate.[2]

---

<sup>4</sup>The condition where oil and gas wells maintain their structural integrity, preventing leaks and ensuring safe and efficient production.

- Traditional modeling approaches, such as dual-porosity models, often oversimplify the behavior of fractured reservoirs. These models do not adequately account for the complex interplay between faults and fractures. More advanced modeling techniques, like Discrete Fracture Network (DFN) models, consider the individual characteristics of faults and fractures, including their spatial distribution, connectivity, and conductivity. These models provide a more accurate representation of fluid flow and pressure behavior in fractured reservoirs.[2]
- The pressure transient behavior in fractured reservoirs is predominantly controlled by the properties of fractures, such as their distribution, connectivity, and conductivity. Faults play a crucial role in this behavior by creating high-permeability zones and influencing fluid flow patterns. Accurate modeling of pressure transient behavior requires considering the contributions of faults. Faults intersecting the wellbore can dominate the pressure behavior, impacting the interpretation of well test data.[2]
- **Exploration Targeting:** Faults can manifest as scarps, lineaments, or seismic abnormalities on both the surface and beneath the ground. These traits can be utilized as exploration markers to identify probable petroleum deposits.[5]
- **Deformation History:** Faults provide insight into a region's tectonic and geological history. Reconstructing a petroleum basin's geological development can help predict hydrocarbon distribution by throwing insight on fault timing and activity.[6]
- **Drilling Process:** Faults play a critical role in the drilling process, impacting both the geological understanding and operational efficiency of drilling activities. Their detection and characterization are essential for ensuring successful drilling and production operations. Faults can compartmentalize reservoirs, affect fluid flow, and pose risks to drilling stability and safety. The detection of faults is crucial for the drilling process to avoid unplanned exits from the pay zone and to prevent fluid losses along fault planes. Geophysical methods, particularly seismic surveys, are commonly used to detect faults. High-resolution seismic data helps in imaging faults, although not all faults can be successfully detected this way. Complementary methods, such as potential field data and surface geology, are also valuable in identifying faults that seismic data might miss.[5]

In horizontal drilling, pre-existing fractures and faults need to be detected in advance. An unexpected fault can act as a thief, causing frac fluids and proppant to leak away from the targeted zone, reducing efficiency and potentially causing induced seismicity. Faults with even small displacements can cause the drill bit to exit the pay zone, necessitating corrections that, if made incorrectly, can result in significant production losses.[5]

Detecting and understanding faults are vital for maintaining operational safety and efficiency. Faults can cause drilling hazards such as wellbore instability and lost circulation. Accurate fault mapping helps in designing

drilling programs that avoid problematic areas, ensuring safer and more efficient operations. This is particularly important in regions with a high density of faults or complex geological settings.[5]

In summary, faults play a central role in the formation, migration, trapping, and production of hydrocarbons within petroleum systems. Geologists and geophysicists study faults extensively to better understand the subsurface dynamics and make informed decisions during exploration and production activities in the oil and gas industry.

### 1.1.1 Overview of the Article: The Role of faults in Hydrocarbon Migration

In this case study, the researchers aimed to challenge the traditional notion of faults as passive barriers to hydrocarbon migration. They conducted numerical simulations in a 2D geological model representing a sedimentary basin with various lithological layers, including source rocks, reservoirs, and seal clays. Within this model, they introduced faults with different permeability levels and behavior (open or sealed) to investigate their role as conduits for hydrocarbon flow.[1]

The simulations focused on faults that are open for relatively short periods, typically lasting thousands of years. This choice allowed the researchers to explore whether such narrow and sporadically open faults could significantly impact hydrocarbon migration within these brief timeframes.[1]

One of the surprising findings was the observation that hydrocarbon velocity in faults originating directly from source rocks can be remarkably high. This result challenges the conventional understanding that active oil seeps can only occur due to leakage from reservoirs. Instead, the study demonstrates that faults linked to source rocks can lead to rapid hydrocarbon movement, even in the absence of permanent fault structures.[1]

Moreover, the efficiency of fault-driven migration was compared to permanent drains in the model. It was revealed that even relatively narrow faults, open for short periods, can be as efficient as permanent drains in filling reservoirs with hydrocarbons. The short-lived permeability of faults was found to be a critical factor in influencing hydrocarbon migration.[1]

The researchers also explored the role of faults in draining hydrocarbons from source rocks, particularly if the source rocks were clay-rich and acted as décollement levels<sup>5</sup>. The simulations showed that such faults can efficiently drain significant quantities of hydrocarbons, regardless of the fault's thickness.[1]

Interestingly, the hydrocarbon velocity and flow within faults were found to be more influenced by the facies the fault connects and the fault/porous network connection rather than the fault itself. Faults that were well-connected with good reservoirs or the surface were observed to serve as highly effective conduits for hydrocarbon movement.[1]

Overall, the study highlights the critical importance of understanding fault behavior and their interactions with the porous network when modeling hydrocarbon migration. The traditional view of faults as mere barriers must be revisited, as

---

<sup>5</sup>Geological horizons along which rocks slide or detach, often associated with fault zones.

even small, intermittently open faults can have a substantial impact on hydrocarbon flow, leading to rapid velocities and efficient migration. Consequently, faults should be carefully considered in hydrocarbon exploration and production studies to obtain a comprehensive understanding of migration processes in sedimentary basins. This research provides valuable insights for the oil and gas industry, helping refine exploration strategies and reservoir management approaches.

## 1.2 Purpose of this Study

The purpose of my research project is to delve into the impact of faults on geomagnetic data. I aim to explore the factors within faults that may give rise to anomalies in magnetic data. Additionally, I intend to examine the correlation between physical observations made in the field and the interpretation of magnetic data. A key objective is to conduct data analysis with utmost precision to minimize noise and errors in the final plots. This precision will facilitate a more accurate and straightforward interpretation of the data.

- **Factors Contributing to the Complexity of Magnetic Anomalies:**
  - **Dipolar Structure of the Magnetic Field:** The Earth's magnetic field acts like a giant dipole magnet, making the analysis of magnetic data more complex.
  - **Multiple Magnetic Sources:** There are multiple magnetic sources within the Earth, all contributing to magnetic anomalies.
- **Impact of Geological and Anthropogenic Noise:**
  - **Geological Noise:** Natural variations in rocks and geological structures can create noise that complicates the interpretation of magnetic data.
  - **Anthropogenic Noise:** Human-made structures such as buildings, power lines, and other infrastructures can also create additional noise.
- **Influence of Induced and Remanent Magnetism:**
  - **Induced Magnetism:** This type of magnetism is created in rocks due to the Earth's magnetic field.
  - **Remanent Magnetism:** This type of magnetism is the leftover magnetism from when the rocks were formed, reflecting changes in the Earth's magnetic field over time.

To validate the notion that variations in magnetic fields can identify faults and fractures in rocks, our study focuses on previously recognized faults. By doing so, we aim to confirm that these magnetic anomalies are indeed associated with faults. Through these efforts, we hope to contribute to a deeper understanding of the complex interplay between faults and magnetic anomalies, ultimately advancing our knowledge of geological processes.



---

## CHAPTER TWO

---

### THEORY

#### 2.1 Understanding Faulting Processes Through Magnetic Properties of Fault Rocks

When a fault occurs, the energy stored in the fault zone is released in three ways: seismic waves (which we can detect with seismographs), breaking of rocks (fracture energy), and heat (frictional energy). The heat generated from friction and the pressure from shearing cause physical and chemical changes in the rocks. These changes affect the grain size, magnetic properties, and mineral composition. Changes in grain size and mineral composition, especially in iron-bearing minerals, also affect the magnetic properties of the rocks.[7]

Tao Yang and his team reviewed and summarized the progress made in studying the magnetic properties of fault rocks. They aimed to explain how and why the magnetic properties of these rocks change and to combine magnetic studies with other scientific methods to get a fuller picture. The paper focuses on how iron minerals in the rocks can reveal important information about the physical and chemical processes that happen during faulting. It also shows how these magnetic properties can indicate stress, temperature changes, and fluid movements in fault zones. The main goal is to better understand faulting by analyzing magnetic properties in detail and using knowledge from different scientific fields.[8]

The researchers focused on iron-bearing minerals in fault rocks because these minerals are sensitive to changes in stress, temperature, and fluids in fault zones. They specifically looked at ferrimagnetic minerals, such as magnetite, hematite, and pyrrhotite, because these minerals retain a magnetic signature even after being subjected to stress or heat from faulting. By studying these minerals, the researchers aimed to understand the magnetic changes that occur in fault rocks.[8]

To conduct their research, the scientists collected samples of fault rocks from various fault zones. These included natural fault zones, where earthquakes have occurred, and synthetic fault rocks created in the lab to simulate fault conditions. Small samples, often just a few milligrams, were then scanned to determine their magnetic properties. This scanning process measured how easily the rocks became magnetized (susceptibility) and how much permanent magnetism they retained (remanence).[8]

The researchers used several types of measurements to analyze the magnetic

properties of the fault rocks:[8]

- **Low-Field Magnetic Susceptibility:** This measurement determines how easily a rock can be magnetized in a weak magnetic field, helping to identify whether the rock contains mostly ferromagnetic minerals, which are strongly magnetic.
- **Frequency-Dependent Susceptibility:** By measuring magnetic susceptibility at different frequencies, the researchers could distinguish between different sizes of magnetic grains.
- **High-Field Magnetic Measurements:** This included measuring hysteresis loops, which show how much of the rock's magnetism remains after an external magnetic field is removed. These measurements help in understanding the magnetic stability and grain size of the minerals.

The researchers also conducted temperature-dependent measurements to gain further insights:[8]

- **High-Temperature Analysis:** By heating the samples, they observed changes in their magnetic properties, which helped identify specific minerals based on their Curie temperatures—the temperatures at which they lose their magnetism.
- **Low-Temperature Analysis:** Cooling the samples to very low temperatures allowed the researchers to identify transitions in magnetic properties, such as the Verwey transition<sup>1</sup> in magnetite.

The study also examined how fluids moving through fault zones and chemical reactions within the rocks affect their magnetic properties. By studying these interactions, the researchers could infer past stress conditions (strain) and temperatures (acting as a geothermometer) in the fault zones. This understanding helps in reconstructing the history of faulting and related earthquake hazards.[8]

Magnetic properties of fault rocks, especially those containing iron minerals, provide valuable insights into faulting processes. These properties are highly sensitive to changes in stress, temperature, and the presence of fluids, making them effective indicators of the physical and chemical processes occurring in fault zones. Examining these magnetic properties allows for a better understanding of the conditions and activities within fault zones.[8]

Several mechanisms influence the magnetic properties of fault rocks, including frictional heating, energy dissipation, and fluid percolation. These mechanisms cause significant changes in the magnetic properties of the rocks, which can be detected and analyzed through detailed magnetic property measurements. Understanding these changes helps trace the history and behavior of faults:[8]

- **Frictional Heating:** During an earthquake, the mechanical energy generated by high seismic slip rates is primarily converted into heat, accounting for about 80% to 90% of the total energy budget. Frictional heating rapidly

---

<sup>1</sup>The Verwey transition is a low-temperature phase transition in the mineral magnetite associated with changes in its magnetic, electrical, and thermal properties.

increases the temperature within the slip zone after a rupture. At shallow depths, the temperature rise may be less than 100°C, but it can exceed 1100°C at seismogenic depths greater than 5 kilometers. This significant temperature rise can induce a variety of thermochemical reactions, including the decomposition and dehydration of mineral phases, leading to the formation of new minerals such as magnetite and hematite. In some cases, the temperature is high enough to cause localized melting of the host rock, resulting in the formation of pseudotachylitesglassy or partially crystallized rocks formed by rapid cooling of the melt.

- **Fluid Percolation:** Fluid percolation through fault zones occurs during the coseismic, postseismic, and interseismic periods. During an earthquake, short-duration pulses of hot fluids, generated by frictional heating, can dissolve preexisting iron-bearing minerals such as pyrite and siderite, releasing  $\text{Fe}^{2+}$  ions. In the postseismic period, these fluids cool down and ferrimagnetic minerals precipitate due to the low solubility of iron oxides and hydroxides at lower temperatures. During the interseismic period, long-term fluid infiltration from meteoric or deeper sources can lead to continuous chemical alterations, including the dissolution and precipitation of magnetic minerals, further modifying the magnetic properties of the fault zone

Magnetic studies have significant potential in uncovering microscopic processes in fault zones that are otherwise difficult to detect. Magnetic properties can serve as tools for analyzing strain, temperature trends, and fluid-rock interactions in fault zones. These studies provide unique insights into the conditions and processes within faults, which are essential for understanding earthquake mechanics and associated hazards.[8]

Magnetic properties of fault rocks are crucial for understanding faulting processes. More detailed and interdisciplinary research is needed to fully unravel the complexities involved. Magnetic studies, combined with other scientific methods, provide a powerful approach to studying the dynamics of fault zones and improving our understanding of earthquake mechanics.[8]

## 2.2 Geomagnetic Method to Identify Faults and Lineaments

Geomagnetic methods are commonly used in geophysics to detect and study lineaments and faults in the Earth's subsurface. Lineaments refer to linear features on the Earth's surface or within the crust, which can include faults, fractures, and other tectonic features. Faults, on the other hand, are specific types of lineaments that represent fractures along which movement has occurred between blocks of the Earth's crust.

When rocks contain magnetic minerals, they acquire a remanent magnetization, which means they retain a record of the past geomagnetic field direction. Additionally, some rocks may acquire induced magnetization when exposed to an external magnetic field. These magnetic properties create variations in the Earth's magnetic field, which can be measured and used for geophysical exploration.

The detection of lineaments and faults using geomagnetic methods relies on the fact that certain geological structures can have different magnetic properties compared to their surroundings. This leads to localized variations in the Earth's magnetic field, which can be mapped and analyzed to infer subsurface features.

Here's how geomagnetic methods aid in detecting lineaments and faults:

- **Magnetic Anomalies:** Lineaments and faults often create disruptions in the Earth's magnetic field due to variations in magnetic properties. Magnetic anomalies are deviations from the expected or regional magnetic field values and are indicative of underlying geological structures. By measuring and mapping these anomalies, geophysicists can identify the presence of lineaments and faults.
- **Semiautomatic Filtering:** semiautomatic filtering techniques based on derivatives of the magnetic data can be applied to enhance the detection of lineaments and faults. These filtering techniques help emphasize specific magnetic signatures associated with subsurface structures, making it easier to interpret and locate lineaments and faults.
- **Wavelength and Wavelet Filters:** The use of wavelength and wavelet filters, applied through discrete Fourier-transform algorithms, can further aid in separating the contributions of shallow surface geology and deeper tectonic structures. This can provide a clearer picture of the subsurface and help identify lineaments and faults that might be concealed by other magnetic signals.
- **Dipolar Nature:** Faults and lineaments can generate complex magnetic anomalies due to their dipolar nature. The interaction between different magnetic domains in the rocks along the faults can create distinct magnetic patterns that are indicative of faulting.

Despite the potential of geomagnetic methods, it's important to acknowledge the complexity of interpreting magnetic data. The superposition of multiple magnetic sources, geological and cultural noise, and the shape of magnetic anomalies can all pose challenges in accurately identifying and characterizing lineaments and faults. Therefore, careful data processing and interpretation are necessary to extract meaningful geological information from geomagnetic surveys.

## 2.2.1 Methods for Identifying and Analyzing Magnetic Anomalies and their Sources

### 2.2.1.1 Windowed Weighted Correlation (WWC) method

Recent advancements in geomagnetic survey techniques have introduced the Windowed Weighted Correlation (WWC) method, significantly enhancing the detection and analysis of geomagnetic anomalies. The WWC method addresses the limitations of traditional approaches by segmenting geomagnetic data into time-specific windows and applying weighted correlation calculations to detect anomalies with high accuracy and sensitivity.[9]

The methodology involves collecting continuous geomagnetic data, segmenting it into daytime and nighttime windows, and calculating weighted correlations to

identify significant deviations from a reference baseline. This approach reduces the impact of environmental noise and improves the detection of subtle and complex anomalies.[9]

The WWC method boasts a detection accuracy of 0.976 and offers several advantages:[9]

- **High Accuracy and Sensitivity:** Effective in identifying true anomalies and reducing false positives.
- **Day-Night Comparison:** Enhances detection reliability by accounting for environmental variations.
- **Noise Reduction:** Minimizes background noise impact, ensuring significant anomalies are detected.
- **Versatility and Robustness:** Applicable in various geological settings and conditions.
- **Comprehensive Data Foundation:** Facilitates further analysis and research in seismic-magnetic relationships.

In summary, the WWC method represents a significant advancement in geomagnetic anomaly detection. Its integration into this research aims to enhance the understanding of geomagnetic field variations and their implications for fault detection and earthquake prediction. This method's accuracy, sensitivity, and robustness make it a valuable addition to the tools available for geophysical research and practical applications in geology and seismology.[9]

### 2.2.1.2 Aeromagnetic Method in Geophysical Exploration

The aeromagnetic method is a geophysical exploration technique used to map variations in the Earth's magnetic field from the air. This method involves measuring the intensity of the magnetic field using magnetometers mounted on aircraft flying at a constant altitude over a specified area. The use of high-resolution aeromagnetic data has proven to be highly effective in identifying structural features such as faults and fractures. The method's ability to provide detailed and continuous subsurface imaging allows for accurate mapping and characterization of geological structures. [10]

The aeromagnetic method involves several key steps, starting with data acquisition. Magnetometers are installed on an aircraft, which flies over the survey area along predetermined flight paths at a consistent altitude. These magnetometers measure the total magnetic field intensity at regular intervals, capturing high-resolution data across the survey grid. This airborne approach allows for extensive coverage of the survey area in a relatively short period, providing a comprehensive dataset for analysis.[10]

Once the raw magnetic data is collected, it undergoes a series of processing steps to improve accuracy and highlight relevant geological features. Initial corrections are made for diurnal variations, which are daily fluctuations in the Earth's magnetic field, as well as other noise sources that could affect the data quality. Advanced processing techniques, such as the application of derivative filters like

the First Vertical Derivative (FVD), First Horizontal Derivative (FHD), and Tilt Derivative (TDR), are used to enhance the visibility of magnetic anomalies. These filters help to sharpen the edges of magnetic anomalies, making it easier to identify structural deformations. The processed data is then interpreted to detect magnetic anomalies associated with structural features such as lineaments and faults. Analytic signal (AS) maps are particularly useful in this stage, as they highlight variations in magnetization that indicate the presence of significant subsurface structures.[10]

The aeromagnetic method offers several significant advantages that make it a preferred choice for geophysical exploration. One of the primary benefits is its high resolution, which provides detailed spatial data that allows for the detection of subtle magnetic anomalies associated with small-scale geological structures. This level of detail is crucial for accurately mapping and characterizing faults and fractures that might be overlooked in lower resolution surveys.[10]

Additionally, aeromagnetic surveys are capable of penetrating deep into the Earth's crust, providing valuable information about subsurface structures at various depths. This depth penetration is particularly beneficial in regions where direct geological observations are not feasible. Another notable advantage is that aeromagnetic surveys are non-invasive, making them suitable for large-scale geological investigations without causing any disturbance to the surface environment. This non-invasive nature, combined with the ability to cover large areas quickly, ensures that aeromagnetic surveys are both efficient and environmentally friendly.[10]

Moreover, aeromagnetic surveys are relatively cost-effective compared to other geophysical methods. They offer extensive coverage at a lower cost, making them an economical choice for geological studies and resource exploration. The continuous data coverage provided by aeromagnetic surveys ensures comprehensive mapping of the subsurface, which enhances the accuracy of geological interpretations and supports better decision-making in exploration and resource management. Overall, the aeromagnetic method is a vital tool in geophysical exploration, providing essential data for mapping and analyzing subsurface geological structures.[10]

## 2.3 Other Geophysical Methods for Identifying Faults and Fractures

### 2.3.1 Seismic Surveying Overview

This section investigates seismic fault stick interpretation techniques based on the study "The Impact of Seismic Interpretation Methods on the Analysis of Faults." This research provides an in-depth examination of various seismic interpretation methods and their implications on fault analysis workflows. The study underscores the significance of accurately identifying and analyzing faults using seismic data, highlighting issues such as fault shadows caused by velocity variations across geological faults. Correcting these requires updating velocity models to pinpoint slower rocks in the hanging wall, enhancing subsurface imaging accuracy.

Identifying faults through seismic data is critical in geology and petroleum

exploration. This involves analyzing seismic images to detect disruptions or offsets in continuous seismic reflectors, which suggest fault structures beneath the Earth's surface.

### 2.3.1.1 Horizon Interpretation

Horizon interpretation plays a pivotal role in geological exploration and seismic data analysis. It involves identifying and mapping continuous seismic reflectors, known as horizons, within subsurface geological formations. These horizons are crucial for understanding subsurface structures and compositions. The interpretation process starts with acquiring seismic data, processing it, and examining seismic profiles to identify potential horizons. Using specialized software, interpreters mark and connect these points to create detailed maps crucial for structural mapping, fault identification, and understanding geological frameworks.[11]

### 2.3.1.2 Seismic Attributes for Fault Detection

Seismic attributes enhance fault detection capabilities. Attributes such as amplitude, frequency, phase, coherence, and curvature are employed to highlight fault-related features, helping geologists better visualize and identify fault patterns. These attributes are derived from the seismic data, providing quantitative measurements crucial for fault analysis.

### 2.3.1.3 Fault Stick Interpretation

Fault stick interpretation is fundamental in understanding subsurface geological structures. This technique involves visually representing fault surfaces using fault sticks, which detail the orientation, shape, and spatial relationships of faults. It is vital for creating three-dimensional models of fault systems, characterizing fault behaviors, and integrating with other geological data to refine interpretations. This technique supports various applications including hydrocarbon exploration and seismic risk assessment.[6]

### 2.3.1.4 3D Fault Interpretation

For a more holistic understanding of fault systems, 3D fault interpretation is utilized. This involves integrating interpretations from multiple seismic sections into a coherent 3D model, allowing geologists to gain comprehensive insights into fault structures and their relationships in three-dimensional space.

The methods discussed, including horizon interpretation, seismic attributes, fault stick interpretation, and 3D modeling, contribute extensively to a thorough understanding of fault structures. These techniques are essential for reliable geological assessments, reservoir characterization, and predicting fluid flow in subsurface environments. Accurate fault identification and interpretation are critical for various geological and industrial applications, underlining the importance of advanced seismic surveying techniques in contemporary geoscience and petroleum studies.

### 2.3.2 Geoelectric Data

Geoelectric data, a subset of geophysical data, offer significant insights into the Earth's subsurface by examining the electrical resistivity of geological materials. This technique serves as a powerful tool for identifying faults and fractures, as it relies on the fundamental principle that different rock types and geological structures possess varying electrical resistivity values. By assessing how readily materials conduct electrical current, geoscientists can gain valuable information about subsurface features.

Geoelectric surveys involve the strategic placement of electrode pairs on the Earth's surface or within boreholes. One pair of electrodes is used to introduce a known electrical current into the ground, while another pair is used to measure the voltage potential. This process is repeated at multiple locations with different electrode configurations, allowing for the construction of a resistivity profile of the subsurface. These measurements are key to detecting geological heterogeneities, including faults and fractures.

Faults and fractures often serve as conduits for groundwater flow and may contain dissolved ions that enhance electrical conductivity. As a result, these subsurface structures tend to exhibit lower resistivity compared to the surrounding rocks. Geoelectric surveys can effectively detect these low-resistivity zones, making them instrumental in pinpointing the locations of faults and fractures beneath the Earth's surface.

Advanced geoelectric imaging techniques, such as electrical resistivity tomography (ERT) and induced polarization (IP), further enhance the identification of faults and fractures. ERT, for example, gathers data from several locations to produce a comprehensive resistivity model of the subsurface. This model can reveal the geometry and extent of fault zones, providing a three-dimensional understanding of these subsurface features. Meanwhile, IP measurements can offer insights into the presence of clay minerals or mineral alterations commonly associated with fault zones, adding depth to fault identification.

In addition to pinpointing fault and fracture locations, geoelectric surveys can estimate the depth of these subsurface structures. By analyzing resistivity data collected at varying electrode spacings, geoscientists can differentiate between shallow and deeper fault zones. This depth profiling is critical for understanding the vertical distribution of faults and fractures within the Earth's subsurface.

Geoelectric data are often integrated with other geological and geophysical datasets, such as seismic data or borehole information. This multi-method approach significantly enhances the accuracy of fault and fracture identification and contributes to the development of a comprehensive subsurface model. Such integrated data are valuable not only for geological studies but also for environmental assessments, civil engineering projects, and groundwater investigations. They assist in mitigating risks associated with subsurface structures and play a pivotal role in diverse applications, ranging from resource exploration to the assessment of construction feasibility and environmental impact.

## 2.4 Høybakken Area: Geological and Tectonic Overview

The Høybakken area, located in central Norway, is a significant region for understanding the tectonic evolution of the Scandinavian Caledonides. This area is characterized by the Høybakken detachment zone and its interaction with the MøreTrøndelag Fault Complex, providing a unique opportunity to study the processes of extension, strike-slip deformation, and the overall tectonic disintegration of an orogen.[12] (see figure 2.4.1)

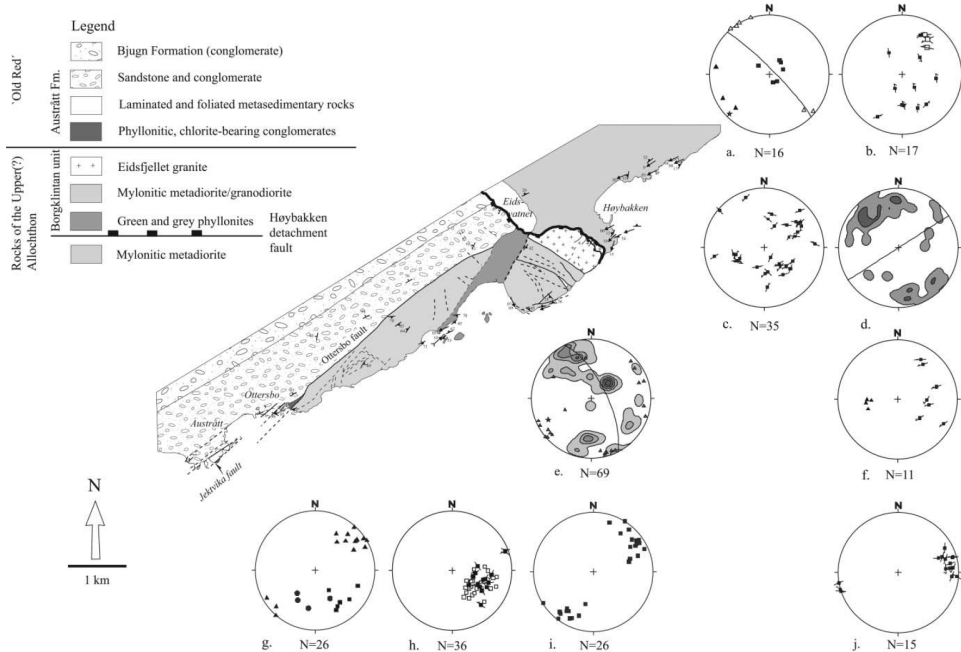


**Figure 2.4.1:** Geological map of the Høybakken area, detailing the distribution of geological units and structural features. This map highlights the location of the Høybakken detachment fault and its interactions with surrounding rock units and fault systems [12].

The interaction between the Høybakken detachment fault and the Møre-Trøndelag Fault Complex is crucial. The detachment fault cuts previously folded detachment mylonites, capturing them in its hanging wall, and the fault system has been influenced by sinistral shearing and various deformation phases. The region exhibits a range of fault types, including normal, oblique, and strike-slip faults, indicating complex tectonic activity.[12](see figure 2.4.2)

The Høybakken detachment fault is characterized by a diverse geological makeup, involving both ductile and brittle deformation processes. Key geological components include:[12]

- **Footwall Geology:** The footwall primarily comprises medium-grade L>S tectonites, predominantly orthogneisses, which show minimal non-coaxial deformation. These rocks include infolded garnet-kyanite-bearing paragneisses, often migmatitic in nature.
- **Detachment Mylonites:** These mylonites represent various protoliths, including meta-dioritic lithologies from the Køli Nappes and paragneisses

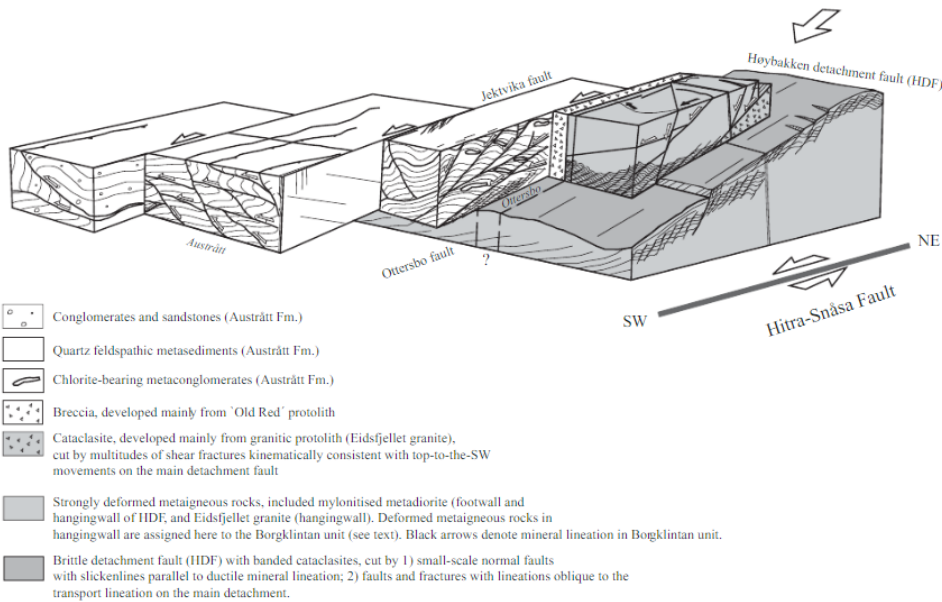


**Figure 2.4.2:** Schematic block diagram showing relationships between structural elements observed in the hanging wall of the Høybakken detachment fault in the Høybakken-Austrått area. This diagram illustrates the interaction between the Høybakken detachment fault and NE-SW trending faults of the Møre-Trøndelag Fault Complex.[12]

and marbles of the Seve Nappe. The degree of mylonitization varies, ranging from protomylonitic to mylonitic grades.

The structural evolution of the Høybakken detachment fault involves both ductile and brittle deformation:[12]

- **Ductile Deformation:** The detachment zone initially experienced significant ductile extensional shearing, leading to the formation of mylonites. This phase was characterized by top-to-the-SW shear sense, indicative of the exhumation processes.
- **Brittle Deformation:** As exhumation progressed, the deformation transitioned from ductile to brittle. The detachment fault itself is sharply defined, displaying outcrop-scale undulations or corrugations that plunge southwestward at an angle of 10-20 degrees. This brittle deformation includes the development of banded cataclasites, ultracataclasites, and brown cataclasites along the fault plane.

The Høybakken detachment fault is oriented with a southwestward plunge, displaying significant undulations along its fault plane. Kinematic analysis reveals several important features, including a SW-NE elongation trend consistent with the ductile structures observed in the footwall and the SW-plunging grooves and undulations on the fault plane. Additionally, an NW-SE-trending slickenside and mineral fiber lineation overlay the fault's corrugations, indicating a late-stage deformation event.[12]

The Høybakken detachment fault exhibits complex interactions with the Møre-Trøndelag Fault Complex, marked by significant structural intricacies. This interaction

includes cross-cutting relationships where the detachment fault cuts through previously folded detachment mylonites, capturing them in its hanging wall. Furthermore, the MøreTrøndelag Fault Complex influences the structural characteristics of the detachment fault, with mutual cross-cutting relationships indicating multiple phases of deformation.[12](see figure 2.4.2)

The hanging wall of the Høybakken detachment fault exhibits a variety of rock types and structural features. It is dominated by the meta-igneous rocks of the Borgklintan unit, including the Eidsfjellet granite. Northward, the hanging wall transitions to sedimentary rocks of the 'Old Red' Bjugn basin. The transition zone between the footwall and hanging wall is marked by banded cataclasites, ultracataclasites, and brown cataclasites, indicating complex deformation processes.[12]

Several significant faults and fractures are associated with the Høybakken detachment fault. Notably, the Ottersbo and Jektvika faults exhibit significant ductile-to-brittle deformation. These faults feature epidote-bearing cataclasite zones and multilayered fault rock sequences, highlighting the intricate interplay of geological forces in this region.[12]

The Scandinavian Caledonides formed due to the collision between Laurentia and Baltica during the Late Silurian to Early Devonian, known as the Scandian orogeny. The region features a complex assembly of Baltic basement-cover slices and exotic terranes thrust southeastwards across the Baltoscandian margin. The geological framework of the Høybakken area is dominated by:[12]

- **The Central Norway Basement Window:** Exposes amphibolite-facies orthogneisses and infolded supracrustal rocks, resembling a metamorphic core complex.
- **The Upper and Uppermost Allochthons:** Include nappes and sedimentary rocks from various geological periods.
- **'Old Red' Basin:** Sedimentary rocks of Devonian age, recording the syn-orogenic and post-orogenic sedimentation history.

The Høybakken detachment zone is crucial for understanding the extensional tectonics that followed the peak of the Caledonian orogeny. It features:[12]

- **Ductile to Brittle Transition:** The zone exhibits a transition from ductile extensional shearing at deeper levels to brittle faulting at shallower levels.
- **Detachment Mylonites:** These rocks, characterized by top-to-the-SW extensional shearing, are found at various structural levels within the detachment zone.
- **Exhumation History:** The exhumation of the Central Norway basement window involved progressive strain localization and cooling from amphibolite-facies to brittle conditions.

The structural evolution of the Høybakken detachment zone involves several key processes:[12]

- **Early Extensional Shearing:** Early to Mid-Devonian extensional shearing led to the exhumation of basement rocks, forming mylonites with top-to-the-SW shear sense.

- **Formation of Extension-Parallel Folds:** Continued extension and exhumation resulted in the formation of folds parallel to the direction of extension.
- **Brittle Detachment Faulting:** The Høybakken detachment fault developed as a brittle fault, truncating previously formed ductile structures and folds.

The MøreTrøndelag Fault Complex plays a significant role in accommodating the deformation within the region. It is characterized by:[12]

- **Sinistral Strike-Slip Faulting:** The fault complex exhibits left-lateral (sinistral) strike-slip movements, which were essential in accommodating the extensional deformation of the region.
- **Flower Structures:** The interaction between strike-slip and extensional processes led to the formation of positive flower structures, indicative of constrictional strain regimes.
- **Cross-Cutting Relationships:** The fault complex shows mutual cross-cutting relationships with the Høybakken detachment fault, indicating a complex interplay between different phases of deformation.

The study of the Høybakken area provides insights into several geological processes. It exemplifies how extensional tectonics can dominate the post-orogenic evolution of a region, leading to significant exhumation and cooling of deep-seated rocks. The coexistence of extensional, strike-slip, and shortening structures highlights the importance of strain partitioning in the tectonic evolution of orogens. Additionally, the adjacent 'Old Red' basins record sedimentation linked to the extensional and exhumation history of the region, providing a valuable record of the late-stage evolution of the Caledonides.[12]

The detailed study of this area not only enhances our understanding of the region's geological history but also provides analogues for similar tectonic settings worldwide. The integration of structural geology, geochronology, and field observations is essential for unraveling the intricate history recorded in the rocks of the Høybakken detachment zone and the MøreTrøndelag Fault Complex.



---

CHAPTER  
**THREE**

---

METHODS

### **3.1 Research Objective and Hypotheses**

The complexity of processing and understanding magnetic anomalies arises from several factors, including the dipolar structure of the Earth's magnetic field and the presence of multiple magnetic sources. Additionally, geological and anthropogenic noise further complicates the interpretation of magnetic data. The shape of magnetic anomalies is influenced by both induced and remanent magnetism, making interpretation even more challenging. Despite these challenges, the magnetic properties of fault rocks provide valuable insights into faulting processes. However, relatively few studies have focused on the magnetic properties of fractured rocks. Comparative studies have shown broad agreement between magnetic and non-magnetic methods, significantly enhancing our understanding of the magnetic signatures of fractured rocks.

#### **3.1.1 Hypotheses**

- Identification of Faults Using Geomagnetic Methods: The first hypothesis addresses whether geomagnetic surveys can effectively identify faults. If there is a significant correlation between magnetic anomalies and fault locations, it would support the use of geomagnetic methods for fault detection in geological surveys.
- Impact of Faults on Magnetic Field Diagrams: The second hypothesis examines the extent to which faults alter magnetic field diagrams. Detectable patterns such as steps, peaks, or troughs in magnetic data can indicate the presence of faults and provide insights into the faulting process.
- Causes of Magnetic Anomalies in Fault Zones: The third hypothesis explores the reasons behind magnetic anomalies in fault zones. Specific faulting processes, such as thermochemical reactions, post-seismic fluid migration, and mechanical reorganization of magnetic minerals, can cause these anomalies. Understanding these processes can improve the interpretation of magnetic data and our knowledge of fault zone dynamics.

This research aims to answer the following key questions:

- Can we identify faults using geomagnetic methods?
- How do faults affect magnetic field diagrams?
- What are the reasons for magnetic anomalies in fault zones?

By addressing these questions, the study will contribute to the field of geophysics by improving the techniques for fault detection and enhancing our understanding of the impact of faulting processes on the magnetic properties of rocks.

## 3.2 Magnetic Surveying Equipment

### 3.2.1 Description of Magnetometer



**Figure 3.2.1:** G-859AP Mining Magnetometer

The G-859AP Mining Magnetometer, produced by the Geometric Company, represents a critical instrument in our geophysical research initiatives. This sophisticated magnetometer demonstrates remarkable speed and efficiency, thereby serving as an indispensable resource in our efforts to detect fault signals within geophysical data. Emphasizing the key features and capabilities of the G-859AP is essential, as they have substantially contributed to the success of our research endeavors.

**Versatile Application in Geological Contexts:** The G-859AP is meticulously designed for geological applications, tailored to the exploration of minerals, oil/gas reserves, diamond deposits, and the comprehensive study of geological

structures. Its versatility aligns seamlessly with the multifaceted demands of our research within the Høybakken detachment zone in Norway.[13]

**GPS Integration and Enhanced Positional Accuracy:** A notable hallmark of the G-859AP is its integration with the NovAtel Smart V1 (1Hz) GPS system. This integration enables the simultaneous recording of latitude and longitude data alongside magnetic readings during our surveys. Furthermore, the potential for user upgrades to the PVT or VBS system promises improved speed and accuracy, a vital consideration in our data collection efforts.[13]

**Efficiency and Real-time Monitoring:** The magnetometer provides continuous surveying capabilities, recording data at user-selectable rates of up to 5 readings per second. This efficiency is particularly advantageous for our brisk walking pace surveys, significantly expanding our ground coverage and ensuring no potential targets are missed. Real-time analog waterfall displays of magnetometer readings and "Quick Look" functionality allow for on-the-fly quality control and the identification of anomalies.[13]

**Data Editing and Versatility:** The G-859AP empowers us with the ability to edit X-Y positions and magnetometer data both in the field and during post-processing. This flexibility not only streamlines data collection but also affords us greater control over the integrity of our data.[13]

**Integration with Powerful Software:** The comprehensive software package accompanying the magnetometer is instrumental in our research efforts. It facilitates the download, editing, and interpolation of magnetic data into 2D or 3D contour-ready formats. This software also enables the rapid production of annotated color maps, providing immediate visualizations following data transfer to our base computer.[13]

**Alignment with Research Objectives:** In light of our research objectives to understand the magnetic response of the Ottersbo fault within the Høybakken detachment zone, the G-859AP has proven to be a reliable and versatile companion. Its capacity to simultaneously capture positional data and magnetic readings, coupled with real-time monitoring and editing capabilities, aligns seamlessly with our mission to identify fault signals and variations in geophysical data.[13]

In summary, the G-859AP Mining Mag serves as an invaluable asset in our geophysical research endeavors, offering efficiency, accuracy, and versatility. Its integration with GPS, real-time monitoring features, and data editing capabilities have played a pivotal role in advancing our understanding of fault signals in geophysical data within the Høybakken detachment zone.

In addition to the G-859AP Mining Mag magnetometer used for detailed geophysical surveys, a constant magnetometer was employed to measure the base magnetic field in the study area. This measurement of the base magnetic field serves as a crucial reference point and baseline against which magnetic anomalies were detected and analyzed.

The constant magnetometer used for this purpose was selected for its stability and reliability in providing accurate measurements of the Earth's magnetic field. Its primary role was to establish a consistent magnetic field reading unaffected by geological anomalies, ensuring that any deviations observed by the G-859AP magnetometer were attributable to local variations, such as those induced by fault structures.

This approach of measuring the base magnetic field enables a clear differen-

tiation between natural variations in the Earth's magnetic field and anomalies generated by geological features like faults. By establishing a reliable baseline, we can confidently identify and interpret the magnetic signatures associated with fault signals in our geophysical data.

The combination of the G-859AP Mining Mag for detailed magnetic surveys and the constant magnetometer for base field measurements provides a comprehensive and robust framework for our research. It allows us to discern subtle variations in magnetic data and gain deeper insights into the geological characteristics of the Høybakken detachment zone.

The integration of these two magnetometers, each serving a distinct yet complementary role, underscores the rigor and precision of our methodology in the pursuit of understanding fault signals within geophysical data in this complex geological setting.

### 3.3 Selection of Study Area

The process of identifying fault signals in geophysical data begins with a deliberate and strategic selection of the survey area. This section outlines the considerations and rationale behind the choice of our survey location within the Høybakken detachment zone in central Norway.

- **Geological Significance:** The Høybakken detachment zone, situated within the broader context of the Scandinavian Caledonides, presents a geological landscape of paramount significance. Characterized by a complex history of extension, strike-slip movement, and shortening, this zone has attracted extensive geological scrutiny over the years. Our research aims to contribute to this understanding by focusing on a specific geological feature within this detachment zone.[12]
- **Scientific Objectives:** Our scientific objectives, as outlined in the research proposal, guided the selection of the survey area. By concentrating our efforts on the Høybakken detachment zone, we aimed to achieve the following:
  - **Enhance fault detection techniques:** We sought to improve our ability to detect and characterize fault signals within geomagnetic data by studying a fault structure known for its complexity and geological significance.
  - **Magnetic field variation analysis:** Our goal was to analyze and interpret variations in magnetic fields on both sides of the fault, shedding light on the fault's geological attributes and magnetic response
- **Practical Considerations:** Practical considerations also played a pivotal role in determining our survey area. These considerations encompassed logistical aspects, accessibility, safety, and the feasibility of conducting fieldwork in the chosen location. The Høybakken detachment zone offered a balance between geological relevance and practicality, making it a suitable site for our research.

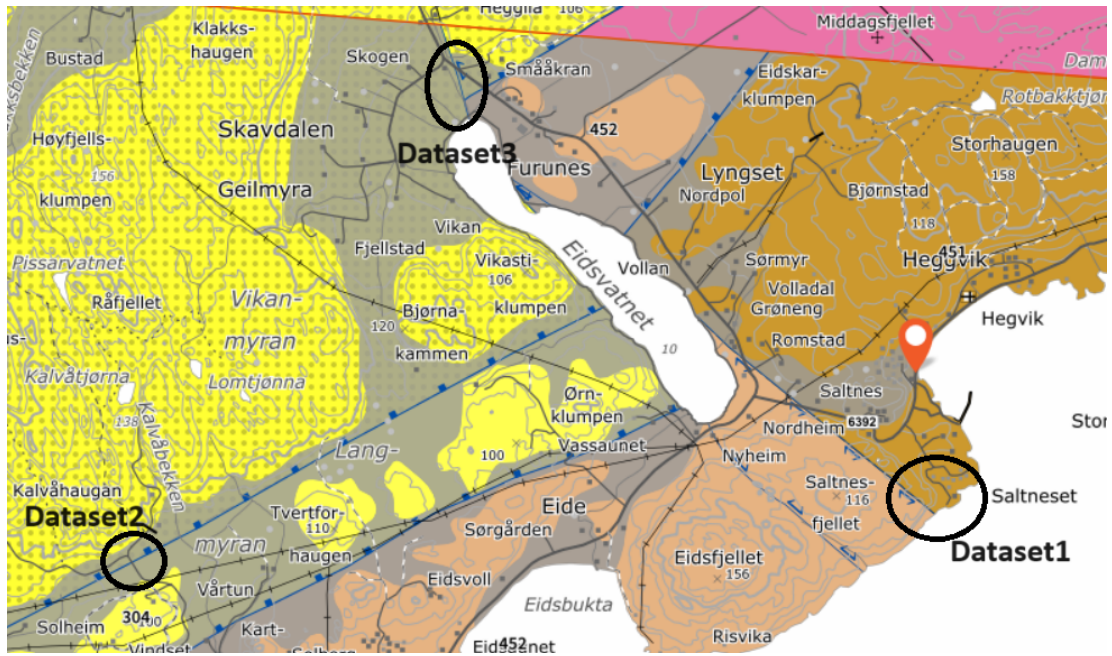


**Figure 3.3.1:** Geological map showing the locations of Dataset 1, Dataset 2, and Dataset 3 within the Høybakken area. Dataset 1 is located near Hegvik, close to the coast, characterized by meta-igneous rocks and sedimentary deposits. Dataset 2 is positioned within the transition zone between the footwall and hanging wall of the Høybakken detachment fault, notable for its banded cataclasites and ultracataclasites. Dataset 3 is situated near the intersection of the Høybakken detachment fault with the Møre-Trøndelag Fault Complex, an area marked by complex fault interactions and diverse lithologies. [14]

### 3.3.0.1 Location of Datasets

**Dataset1:** Dataset 1 is located in the Høybakken area near the coast at Hegvik. This area is characterized by its proximity to the Høybakken detachment fault, making it an ideal location for studying the geological and structural features associated with this fault zone. The geology of this region includes a mix of meta-igneous rocks of the Borgklintan unit and the sedimentary rocks of the 'Old Red' Bjugn basin. The specific coordinates place Dataset 1 in an area where significant ductile-to-brittle deformation has been observed, providing valuable insights into the fault dynamics.[12]

**Dataset2:** Dataset 2 is situated within the transition zone between the footwall and hanging wall of the Høybakken detachment fault. This location is notable for its banded cataclasites, ultracataclasites, and brown cataclasites, indicative of intense deformation processes. The dataset is positioned in an area dominated by orthogneisses and infolded paragneisses from the southwestern Central Norway basement window. The proximity to the Ottersbo fault provides additional context for studying the interactions between different fault structures.

**Dataset3:** Dataset 3 is located near the intersection of the Høybakken detachment fault with the Møre-Trøndelag Fault Complex. This region is marked by significant tectonic activity, including sinistral strike-slip movements and the presence of complex fault interactions. The geology here features a diverse mix of rock types, including meta-dioritic lithologies from the Koli Nappes and paragneisses and marbles of the Seve Nappe. The location of Dataset 3 offers a comprehensive view of the tectonic evolution and structural complexities associated

with the major fault systems in the area.

These datasets collectively cover key areas of the Høybakken detachment fault, providing a broad spectrum of geological and structural data essential for understanding the fault's dynamics and its interactions with surrounding geological features.

### 3.3.1 Placement of Survey Transects

The strategic placement of survey transects is a pivotal aspect of our geophysical research methodology. To ensure the gathering of precise and significant magnetic data, a number of parameters must be carefully taken into account. In this section, we elucidate the rationale behind the placement of survey transects, taking into account both the base magnetometer and the wearable backpack-style magnetometer.

To minimize magnetic interference from external sources, particularly residential houses, power cables, and other objects with magnetic properties, we adopted a proactive approach. The placement of the base magnetometer was meticulously planned to be at a considerable distance from such potential sources of magnetic contamination. This distancing was crucial to ensure that the readings obtained from the base magnetometer accurately represented the base magnetic field unaffected by local disruptions.

Accurate positional data is fundamental to our research, given its close correlation with magnetic readings. Hence, the base magnetometer was strategically positioned at an elevated height to optimize GPS accuracy. This elevation not only ensured a clear line of sight for satellite signals but also reduced potential obstructions that might compromise the precision of the GPS system. The reliability of our GPS data is integral to the precise mapping of magnetic variations across the survey transects.

In contrast, the wearable backpack-style magnetometer, the G-859AP, demanded a distinct approach. As this magnetometer requires mobility along the survey transects, we meticulously selected transect locations that minimized unwanted objects or magnetic interferences along the chosen paths. Transects were charted with the aim of providing a relatively obstacle-free trajectory for the wearable magnetometer, ensuring that magnetic data collected during transect surveys were representative of the geological features under investigation.

Throughout the process of transect selection and placement, safety considerations were paramount. The avoidance of hazardous terrain and adherence to safety protocols were non-negotiable. Moreover, the placement of transects and magnetometers was designed to maximize data integrity and minimize potential risks.

It is essential to emphasize that the placement of survey transects was guided by our overarching research objectives. These objectives revolved around the identification of fault signals in geophysical data within the Høybakken detachment zone. Thus, the placement of transects was a deliberate effort to capture magnetic variations and anomalies relevant to fault structures.

In conclusion, the strategic placement of survey transects played a fundamental role in our research methodology. It reflects a careful balance between mitigating magnetic interference, optimizing GPS accuracy, ensuring safety, and aligning

with our research goals. This meticulous planning and execution are central to the integrity and reliability of our geophysical data, ultimately contributing to the success of our study in identifying fault signals within the Høybakken detachment zone.

## 3.4 Data Collection

In this section, we outline the methodology employed to gather magnetic field data within the chosen survey area, with a focus on the Ottersbo fault within the Høybakken detachment zone. The data collection process involved the use of two distinct magnetometers: a base magnetometer strategically placed for reference measurements and a wearable magnetometer (G-859AP) for transect surveys.

### 3.4.1 Magnetic Field Measurements

Our magnetic field data collection relied on two primary instruments:

- **Base Magnetometer:** We employed a stationary Geometrics magnetometer as the reference instrument. This magnetometer was strategically placed at a fixed location chosen to represent the base magnetic field. It continuously recorded magnetic field measurements unaffected by local disturbances. Continuous magnetic field measurements were recorded by the base magnetometer at a rate of 6 readings per minute. Over time, this constant observation guaranteed a thorough comprehension of the base magnetic field.
- **Wearable Magnetometer (G-859AP):** The G-859AP, a portable magnetometer designed for field surveys, played a central role in our data collection. This backpack-style magnetometer allowed for mobility and was used to traverse designated survey transects. It provided the flexibility needed to collect magnetic data along precise paths. During transect surveys, magnetic measurements were recorded at intervals of 5 readings per second. The sampling strategy aimed to maintain consistent coverage along survey transects while ensuring data integrity.

Both magnetometers were equipped with non-volatile memory storage, allowing collected data to be stored for subsequent analysis.

To ensure accurate georeferencing of magnetic measurements during transect surveys, the G-859AP was equipped with a GPS system (NovAtel Smart V1). The GPS system was configured to record positional data simultaneously with magnetic measurements, facilitating precise mapping of magnetic field variations along the survey transects.

Our fieldwork prioritized safety at all stages. We adhered to established field safety protocols, ensuring the well-being of team members and minimizing potential risks associated with data collection in the field environment.

Upon completing data collection, we retrieved the raw magnetic field data directly from the wearable magnetometer (G-859AP) using the MagMap software. This software allowed us to efficiently download the recorded data and prepare it for subsequent analysis. The downloaded data files were organized and stored for further processing.



**Figure 3.4.1:** Observation of rock's magnetic field on both sides of the fault

In addition to the primary magnetic field measurements, we conducted measurements on rocks located on both sides of the fault using a magnetic field detector. These measurements were aimed at observing variations in the magnetic fields associated with the geological formations adjacent to the fault.

By incorporating these rock sample measurements and visual representations of magnetic field variations, we gained valuable insights into the geological context and magnetic field behavior in proximity to the fault zone. This additional data served to enhance our understanding of the magnetic signals associated with fault structures within the study area.

### 3.4.2 Quality Control and Data Preprocessing

To maintain data quality, we implemented validation procedures during data collection. These procedures included periodic checks for sensor stability, verification of instrument functionality, and identification of potential anomalies in real-time data. Any deviations from expected measurements were noted and addressed promptly. Throughout the data gathering procedure, thorough field notes were taken to give context for the data that was gathered. These notes documented environmental conditions, survey locations, any unexpected observations, and de-

viations from the planned methodology. The field notes served as invaluable references for later data analysis and interpretation.

### 3.4.3 Data Calibration

Prior to initiating data collection, both magnetometers underwent a thorough calibration process to ensure the accuracy of measurements. Calibration procedures involved the adjustment of zero field offsets and validation of sensor orientations to guarantee reliable magnetic data.

## 3.5 Data Processing

### 3.5.1 Correction, Smoothing, and Plotting Magnetic Field Data Over Time

The data processing phase of this research involved rigorous procedures to prepare the datasets for comprehensive analysis. The objective was to reliably test the hypothesis that there is a strong link between magnetic anomalies and geological faults. This required accurate synchronization and integration of time-stamped magnetic field measurements with GPS location data, as well as the application of geophysical corrections and various data smoothing techniques to enhance the signal-to-noise ratio.

The process begins by importing magnetic field, base magnetic field, and GPS data from an Excel file, which was previously converted from a text file. Since the magnetic field data and the base magnetic field data were collected at different time intervals using separate devices, it was necessary to synchronize these datasets. The base magnetic field data serves as a reference or control, providing baseline geomagnetic values that are expected without the influence of local anomalies. By interpolating the magnetic field data to match the time stamps of the base data, a direct comparison could be made, enhancing the accuracy of the anomaly detection.

The next critical step involved merging the interpolated magnetic field data with GPS data. This merging process is essential for spatial analysis, associating each magnetic measurement with a specific geographic location. The integration with GPS data is particularly important when studying geological features, as it allows for the correlation of magnetic anomalies with specific locations on the Earth's surface.

The next step was to remove outliers. Outliers in magnetic field data can arise due to various reasons, such as instrumental errors, external electromagnetic interference, or anomalous geological events not related to the studied fault lines. Removing these outliers helps in refining the data quality, ensuring that the analysis focuses on true geomagnetic anomalies that might indicate the presence of faults.

For each data point, the International Geomagnetic Reference Field (IGRF) model was applied. The IGRF model provides a standardized method to compute the expected geomagnetic field values based on the latitude, longitude, and altitude at a given time. This step required converting the timestamps into a format compatible with the IGRF computation routines. The calculated IGRF values

were then used to correct the raw magnetic field data, subtracting the IGRF value from the observed magnetic field value at each point. This correction is crucial as it removes the global geomagnetic field influence, isolating the local magnetic anomalies which may be associated with geological structures such as faults.

After correcting the data and removing outliers, the magnetic field data was smoothed. Smoothing is applied to reduce noise and fluctuations in time series data, making it easier to identify overarching trends and patterns. This is achieved by averaging the data points within a moving window across the dataset. Smoothing helps in visualizing the data more clearly, highlighting significant changes in the magnetic field that could correlate with geological features.

Finally, the processed data was plotted over time. Visualizing the data is a fundamental analytical step, providing a clear graphical representation of the magnetic field variations over time. This visualization aids in the interpretation of data, allowing for the identification of patterns or anomalies that could be linked to geological structures. The plots serve as a preliminary indication of areas where magnetic anomalies coincide with known faults, thus supporting the hypothesis that there is a strong link between magnetic anomalies and geological faults.

### 3.5.1.1 Dataset1-Interpretation and Implications

During the preliminary analysis, it was observed that there were gaps in the magnetic field datetimes when measurements were not recorded. Identifying these gaps is crucial for ensuring the continuity and reliability of the dataset, especially when analyzing time-series data where temporal consistency is essential.

To address the issue of missing data, interpolation techniques were employed. Interpolation is a statistical method used to estimate missing values based on the range and distribution of known data points. This step is vital for reconstructing the missing segments of the magnetic field data, thus enabling a continuous analysis across the entire time series.

In figure 3.5.1 the sharp drops and subsequent recoveries could indicate magnetic anomalies. These anomalies could be linked to geological structures such as faults, as hypothesized. The specific locations and characteristics of these anomalies could provide insights into the underlying geology, potentially indicating fault lines or other significant geological features.(Fig 3.5.1)

The smoothing applied to the data helps in highlighting the broader trends by filtering out high-frequency noise. This makes it easier to focus on significant changes which are more likely to correlate with geological phenomena.(Fig 3.5.1)

If these anomalies spatially correlate with known faults or other geological data (not shown on this plot), they could substantiate the hypothesis that magnetic anomalies are strongly linked to geological faults. It would be critical to cross-reference these time points with GPS data to locate the anomalies geographically.(Fig 3.5.1)

To fully utilize this data in the research, mapping these time-based anomalies to their respective geographic locations would be essential. This would allow for a direct comparison with geological maps to identify any correlations with fault lines or other relevant features. Integrating this magnetic field data with other geological surveys and data types could enhance the understanding of the observed anomalies.

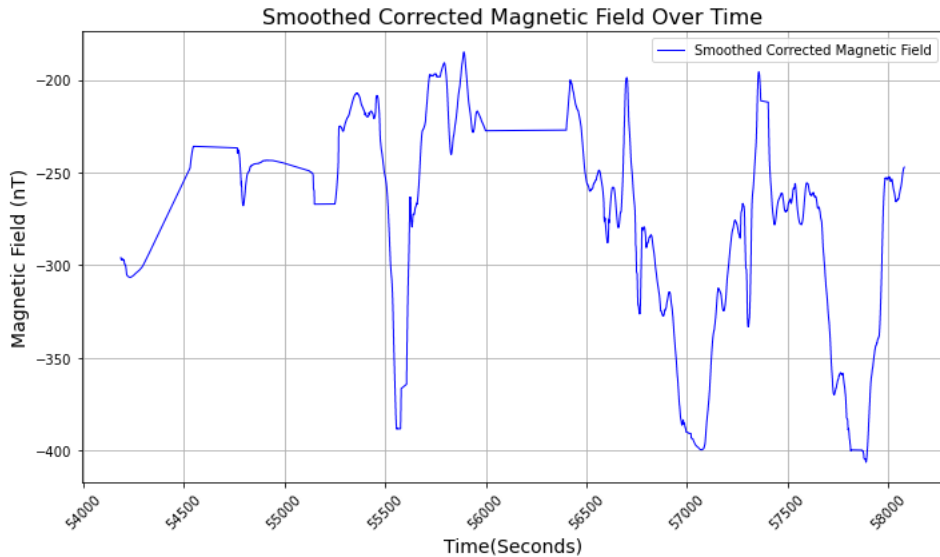


**Figure 3.5.1:** Smoothed Corrected Magnetic Field Over Time. This plot illustrates the variations in the magnetic field strength, measured in nanoTesla (nT), against time in seconds, ranging from 54,000 to 59,000 seconds. Notable features include sharp declines and subsequent recoveries in magnetic field values, suggesting potential geological anomalies. The smoothing of data highlights significant trends while minimizing the impact of high-frequency noise, aiding in the identification of patterns potentially related to underlying geological structures.

### 3.5.1.2 Dataset2-Interpretation and Implications

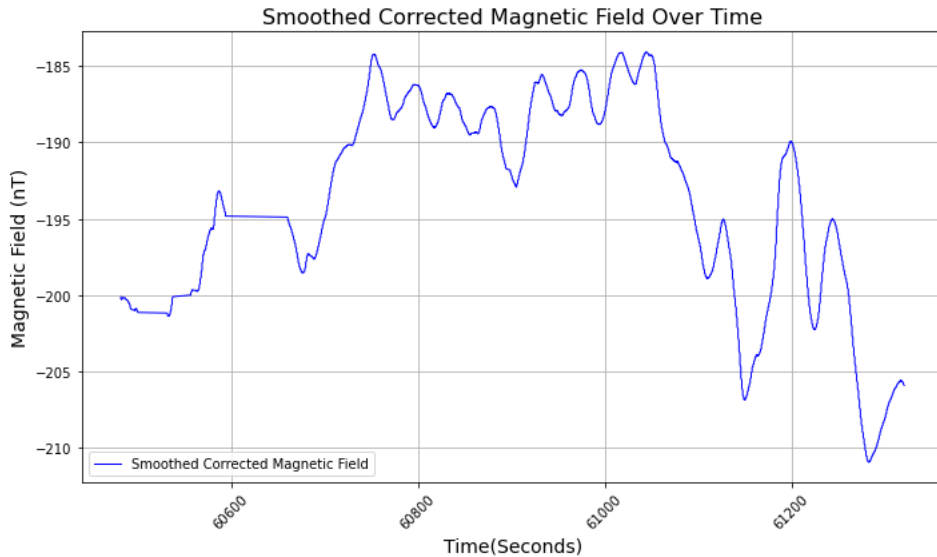
For Dataset 2, a thorough examination was conducted to detect any gaps or missing data points within the magnetic field measurements, similar to the approach taken with Dataset 1. This assessment involved reviewing the continuity of the time-series data and verifying temporal consistency across all recorded measurements. The analysis confirmed that Dataset 2 did not exhibit any missing data, thereby eliminating the need for interpolation techniques used in Dataset 1. This consistency in data capture for Dataset 2 ensures a robust basis for subsequent analysis and interpretation without the necessity for data reconstruction.

Fig 3.5.2 presents the magnetic field strength measured in nanoTesla (nT) over time, plotted from 54,000 to 61,200 seconds. This visualization, which has been smoothed and corrected to reduce noise and extraneous magnetic influences, offers a clear depiction of underlying geological structures through magnetic field variations.

When viewing the graph as a whole, it displays significant fluctuations in magnetic field strength, ranging approximately from -210 nanoTesla to -185 nanoTesla. These variations suggest changes in subsurface geological features which might include differences in rock types, the presence of faults, or other geomagnetic disturbances. The sharp changes, particularly where the magnetic field strength suddenly drops and then recovers, could indicate geological structures like fault zones or transitions between different rock compositions.(Fig 3.5.2

### 3.5.1.3 Dataset3-Interpretation and Implications

The analysis verified that Dataset 3 contains no missing data, thus obviating the need for the interpolation techniques that were necessary for Dataset 1. This



**Figure 3.5.2:** This plot represents the variations in the magnetic field strength, measured in nanoTesla (nT), against time in seconds, ranging from 54,000 to 61,200 seconds. The data displayed has been smoothed and corrected to minimize the influence of noise and non-local magnetic fields, emphasizing significant trends and anomalies.

complete data capture in Dataset 3 provides a solid foundation for further analysis and interpretation, ensuring that no data reconstruction is required.

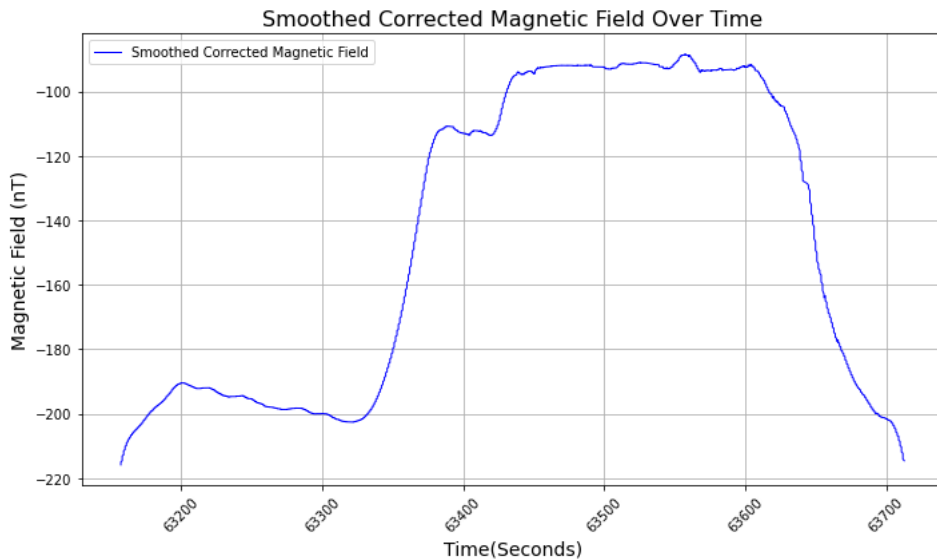


**Figure 3.5.3:** This plot depicts the variations in the magnetic field strength, measured in nanoTesla (nT), against time in seconds, ranging from 53,200 to 57,200 seconds. The magnetic field data has been smoothed and corrected to emphasize significant changes and highlight the overall trends over the observed period.

Figure 3.5.3 displays significant fluctuations in magnetic field strength over time, suggesting notable geological transitions. It begins with a sharp decline, indicating an abrupt entry into a region with different magnetic properties, likely due to a geological boundary or lower magnetic mineral content. This is followed by a gradual increase to a plateau, signifying a traverse through an area with relatively homogeneous geological features. A pronounced peak then suggests a region

enriched with magnetic minerals or a specific geological structure, like an igneous intrusion. The graph concludes with a sharp decline, mirroring the initial drop, possibly marking exit from the high-magnetic region or another significant geological transition. Overall, this pattern illustrates distinct geological zones, each characterized by varying magnetic properties, useful for interpreting subsurface features.(Fig 3.5.3)

In geophysics, variations in the magnetic field can be caused by several factors, primarily geological, due to the different magnetic properties of rocks. For instance:

- **Magnetic Minerals:** Certain minerals, like magnetite, significantly influence local magnetic fields. Areas rich in magnetic minerals will show higher magnetic readings.
- **Faults:** Faults can create magnetic anomalies. When rocks are displaced along a fault, the magnetic minerals within them might align differently, altering the magnetic field.
- **Rock Type Variations:** Different types of rocks have different susceptibilities and remanent magnetization, which can cause local variations in the magnetic field.

Besides geological reasons, other factors can also cause variations in magnetic field measurements:

- **Instrumental Errors:** Malfunctions or inconsistencies in the measuring equipment can produce erroneous data.
- **External Electromagnetic Interference:** Nearby electrical equipment or power lines can interfere with magnetic measurements.
- **Environmental Factors:** Temperature and humidity can affect the sensitivity and performance of magnetic sensors.

Thus, while the observed variations in the magnetic field data are often primarily interpreted as indications of subsurface geological structures, it's crucial to consider and rule out potential non-geological factors that might influence the data to ensure accurate interpretations.

### 3.5.2 Plotting GPS Data and Visualizing Magnetic Field Variations Over Geographic Coordinates

The second step in my data processing involved handling the GPS data, which is crucial for the spatial analysis of magnetic field measurements. I started by loading the GPS data from an Excel file, which contains latitude, longitude, and altitude information corresponding to the timestamps when magnetic data were recorded. Recognizing the potential for GPS errors that could skew my analysis, I promptly applied an outlier removal process. Utilizing the interquartile range (IQR) method, I identified and removed any data points that fell outside the acceptable bounds determined by the first and third quartiles. This step was essential for ensuring

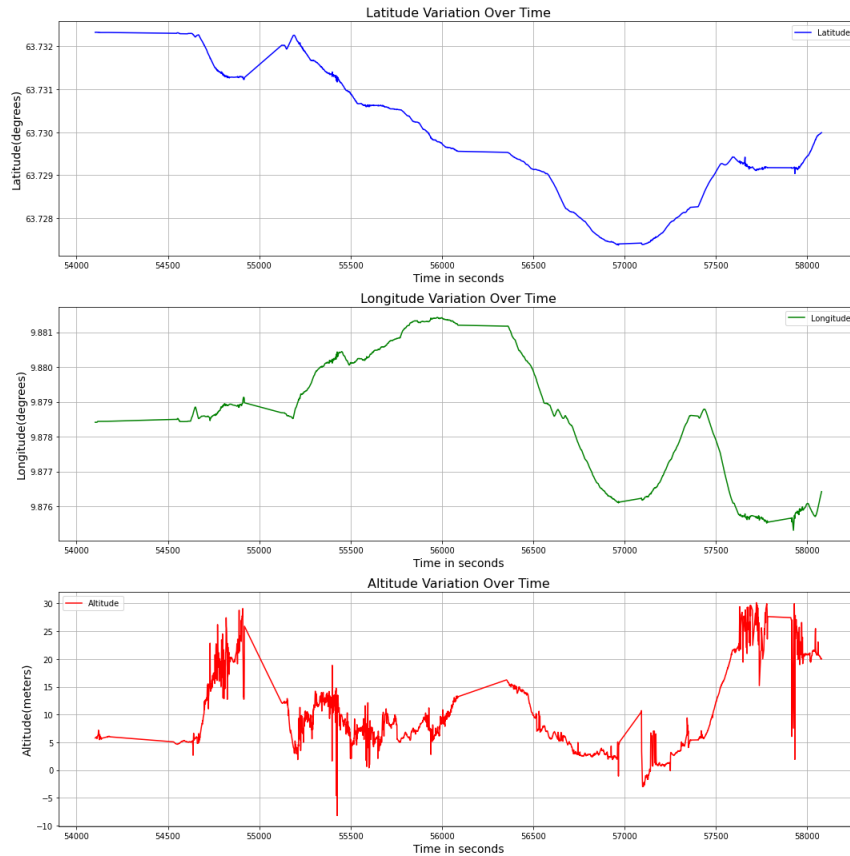


**Figure 3.5.4:** Latitude, Longitude, and Altitude Variation Over Time in Dataset1. This set of three graphs tracks the changes in latitude, longitude, and altitude over time, measured in seconds. The continuous lines represent the paths and elevation changes recorded during data collection, highlighting geographic movements and altitude variations that may influence magnetic field measurements.

the accuracy of my geographic positioning, thereby preventing geographic errors from influencing my interpretation of the magnetic data.

Once the data was cleaned, I faced the challenge of aligning the GPS data with the magnetic field measurements, which were not recorded at identical time intervals. To resolve this, I converted the GPS timestamps into seconds and then set up interpolation functions using SciPy's `interp1d` for latitude, longitude, and altitude. These functions allowed me to interpolate GPS coordinates for each timestamp in the magnetic field dataset, ensuring that every magnetic measurement had a corresponding set of GPS coordinates.

In Dataset 2, the GPS data initially indicated erroneous location details due to a device error during data collection, which led to coordinates being recorded in the incorrect format. This issue was crucial to address because accurate geographic positioning is essential for aligning magnetic field data with specific geological features and ensuring the reliability of the analysis. To resolve this, I developed and implemented a script specifically to convert the GPS coordinates into the correct format. After applying this conversion, the corrected GPS data accurately reflected the actual locations, ensuring that subsequent data analysis would be based on precise geographic positioning. This adjustment was fundamental for the integrity of the dataset and the validity of the associated geological interpretations.

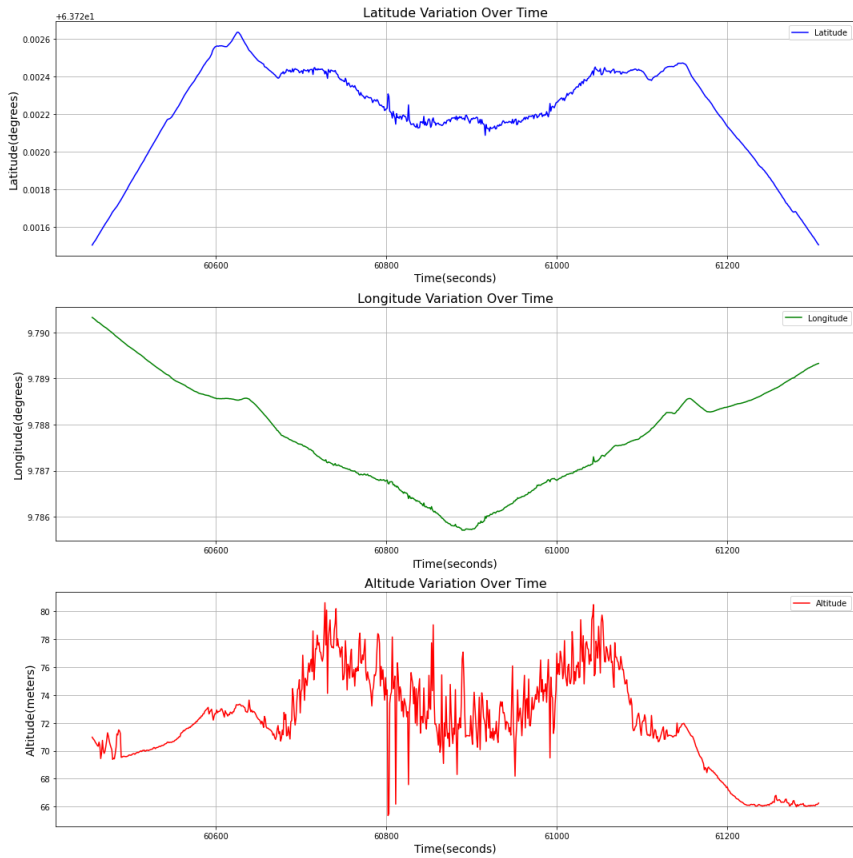


**Figure 3.5.5:** This set of three graphs from dataset2 displays the changes in latitude (top graph), longitude (middle graph), and altitude (bottom graph) over time, measured in seconds from 66,000 to 61,200. These graphs collectively represent the GPS tracking data of a moving object, providing insights into its trajectory and changes in elevation over time.

(Fig 3.5.5)

With the GPS data aligned and interpolated, I moved on to the visualization phase. I created both 2D and 3D plots to visually represent the magnetic field data over the geographic coordinates. In the 3D scatter plot, points were plotted in a space defined by latitude, longitude, and altitude, with each point color-coded based on its corrected magnetic field strength. This visual setup provided a vivid depiction of how magnetic fields varied across different geographic locations. Additionally, I produced a 2D scatter plot that mapped latitude against longitude, again using color to represent magnetic field intensity. This plot was particularly useful for illustrating the path of data collection and highlighting significant magnetic anomalies.

These visualizations are not only crucial for my understanding of spatial patterns in the magnetic data but also serve as compelling evidence of the distribution of magnetic anomalies, which can be directly correlated with geological structures like faults. By combining the cleaned and interpolated GPS data with the magnetic measurements in these visual formats, I can more effectively analyze and present the geographic distribution of magnetic anomalies, enhancing the reliability and clarity of my conclusions regarding the relationship between magnetic anomalies and geological faults.

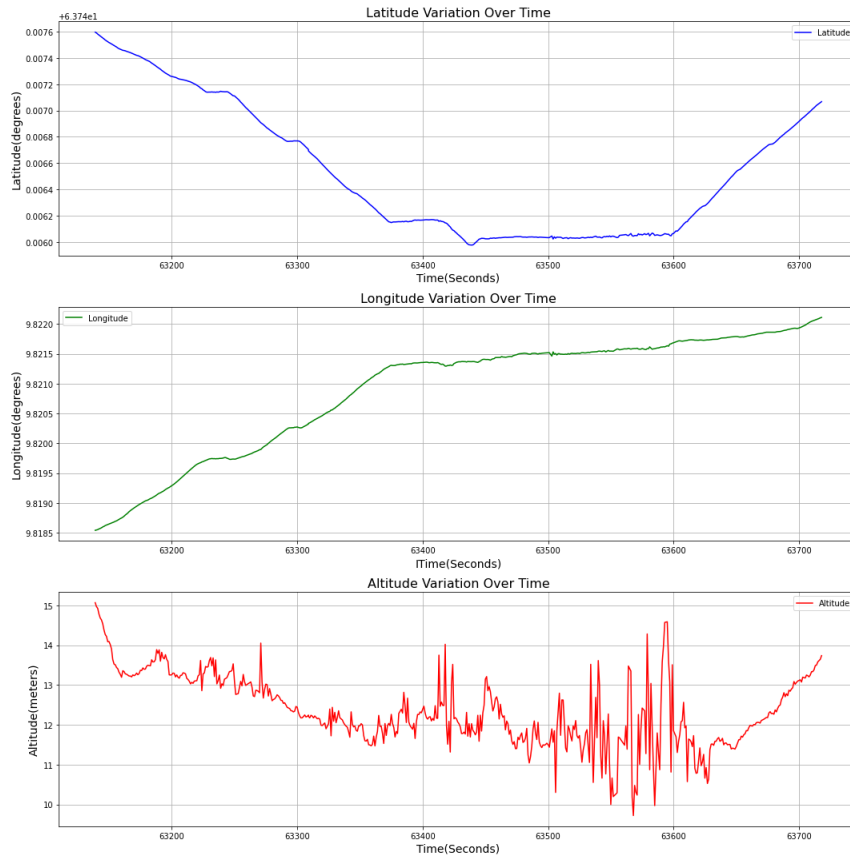


**Figure 3.5.6:** This series of graphs from dataset3 illustrates the changes in GPS coordinates and altitude from time 62,000 to 67,000 seconds. These combined variations help to trace the path and terrain navigated by the subject during the observation period.

### 3.5.3 Geospatial Visualization of Magnetic Field Intensity

In this section, I elaborate on the methods used to visually represent magnetic field data over geographic coordinates, emphasizing the steps involved in transforming raw geospatial data into a meaningful visual context. The goal was to facilitate the understanding of how magnetic field variations correlate with geographic locations, crucial for identifying geological features such as faults.

The visualization process began by structuring the cleaned magnetic field data, which included interpolated GPS coordinates, into a format suitable for geospatial analysis. This involved converting the data into a geospatial data frame, a fundamental step for integrating geographic coordinates with  $\Delta F$  measurements. Each point in the dataset was represented by latitude and longitude coordinates, along with associated  $\Delta F$ .

To ensure the data was accurately represented on a global scale, I set the coordinate reference system (CRS) to WGS84, a standard global reference system used for GPS data. This step is vital as it anchors the dataset to a well-recognized geographic framework, facilitating accurate mapping and spatial analysis.

Following the CRS setup, I converted the data into the Web Mercator projection, a commonly used geographic projection for web mapping services. This transformation was necessary to align the dataset with most online map visuals, which utilize this projection for optimal performance and compatibility.

To highlight specific features in the magnetic field data, I chose to focus on

3D Plot of Corrected Magnetic Field Variation Over GPS Coordinates

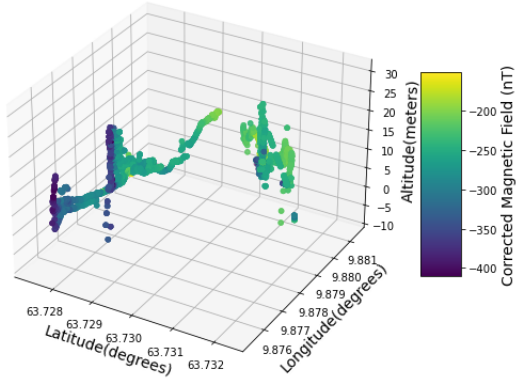


Figure 3.5.7: Dataset1

3D Corrected Magnetic Field Variation Over GPS Coordinates

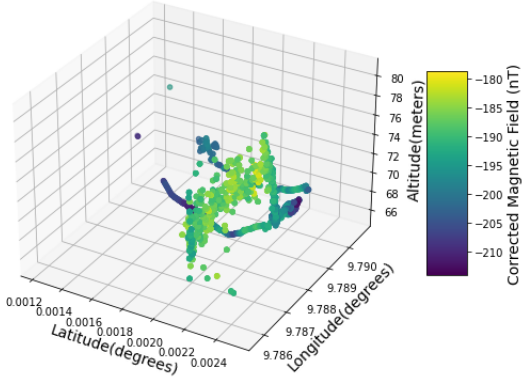


Figure 3.5.8: Dataset2

3D Corrected Magnetic Field Variation Over GPS Coordinates

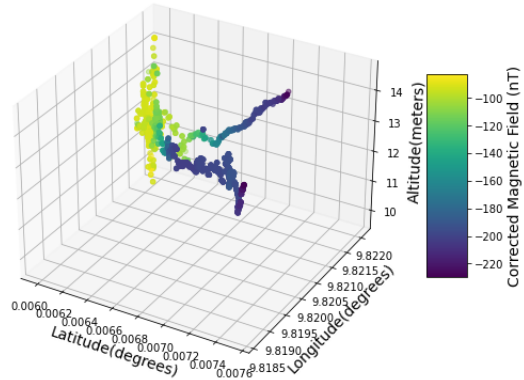
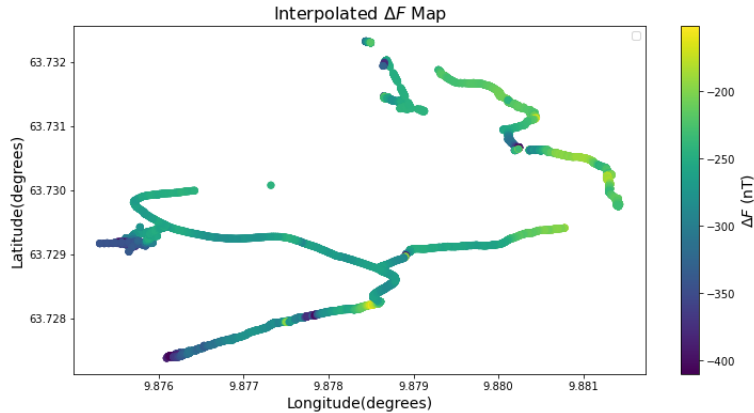
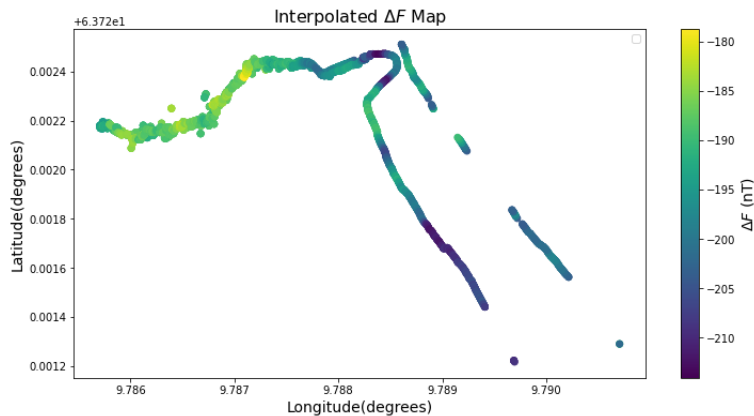


Figure 3.5.9: Dataset3

**Figure 3.5.10:** 3D plots of corrected magnetic field variation over GPS coordinates for three different datasets.



**Figure 3.5.11:** Dataset1



**Figure 3.5.12:** Dataset2

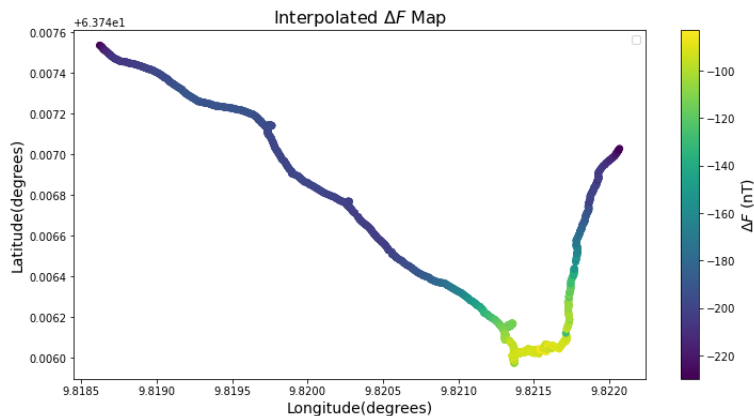


**Figure 3.5.13:** Dataset3

**Figure 3.5.14:** 2D plots of corrected magnetic field variation over GPS coordinates for three different datasets.

a particular range of  $\Delta F$ . By setting visualization limits, I aimed to enhance

the distinction between normal background variations and those anomalies that could indicate significant geological phenomena. This involved normalizing the data's color representation to reflect  $\Delta F$  within a predefined range, making the visualization more intuitive and easier to interpret.

The actual mapping was executed by overlaying the geospatial data points onto a base map sourced from a popular online mapping service. This step not only provided a geographical context to the data points but also enhanced the visual appeal of the analysis, making complex data more accessible and understandable. The integration of a color scale further aided in demystifying the data, allowing for an immediate visual interpretation of  $\Delta F$  across different areas.

Each data point was plotted according to its geographic coordinates and colored based on its corrected magnetic field value, with color intensities representing different levels of magnetic anomalies. This method of visualization not only provided a clear and direct visual representation of the spatial distribution of  $\Delta F$  but also highlighted areas where significant deviations occur, suggesting underlying geological activities.

This approach to geospatial visualization is not merely about creating visually appealing maps but about transforming data into a powerful analytical tool that provides insights into the magnetic properties of the Earth's crust. By correlating specific magnetic anomalies with geographic locations, we can infer the presence and characteristics of underlying geological structures, advancing our understanding of geophysical phenomena.

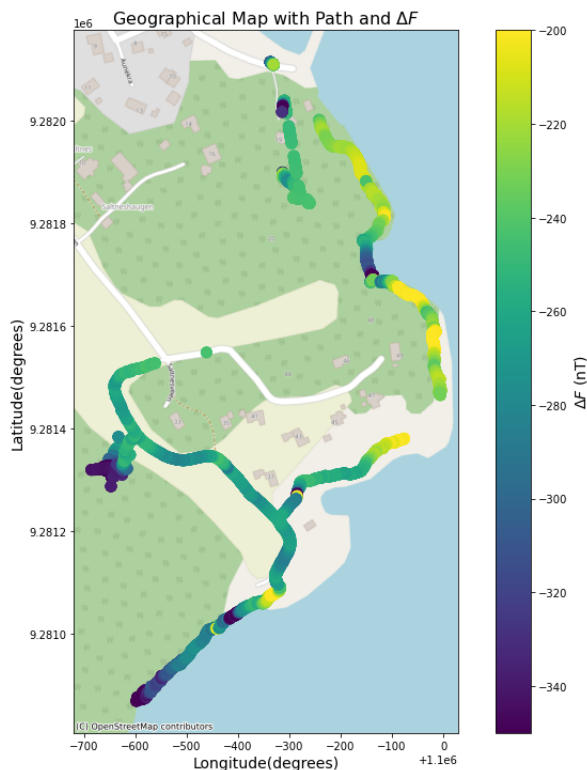


**Figure 3.5.15:** This figure displays the  $\Delta F$  (measured in nanoteslas, nT) along a predefined path on a geographical map (Dataset1). The color gradient represents different intensities of the magnetic field anomalies, ranging from -200 nT to -340 nT.

The data visualized in figure 3.5.15 represents the  $\Delta F$  recorded along a specific

path during a field survey. The path, marked with varying colors from yellow to dark purple, shows significant fluctuations in  $\Delta F$ . These fluctuations can be indicative of underlying geological features such as faults and fractures.

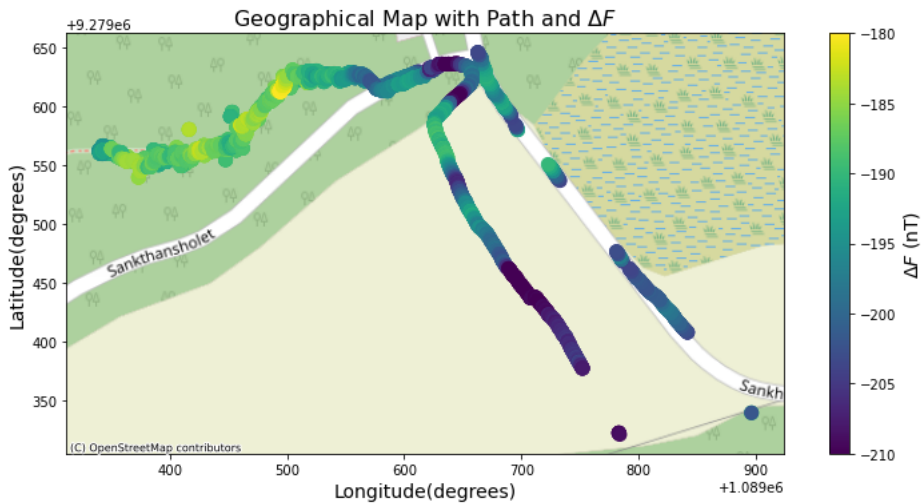


**Figure 3.5.16:** This map illustrates the spatial  $\Delta F$  recorded during the second geomagnetic survey(Dataset2). The color gradient represents  $\Delta F$  measured in nanoteslas (nT), ranging from -180 nT to -210 nT across the surveyed path.

The observed  $\Delta F$  pattern in figure 3.5.16, particularly the areas with the lowest  $\Delta F$  (darkest purple), could be associated with fault zones where rock types and structures vary significantly. This variation can be crucial for identifying fault locations and understanding their orientation and extent.

The stark contrast in  $\Delta F$  along the path in figure 3.5.17, especially where the gradient shifts rapidly, might suggest a boundary between different geological formations or the presence of a fault line. This fault line could act as a barrier or conduit for magnetic minerals, affecting local magnetic field intensity.

Overlaying this data onto a geological map would provide further insights into the correlation between observed magnetic anomalies and specific geological formations. It will be essential to compare these anomalies with geological features like fault lines, lithological boundaries, or areas with known mineral deposits to assess the potential causes of magnetic variation. This comparison can help validate the geomagnetic method's effectiveness in identifying subsurface geological features and enhance the understanding of the area's structural geology.

### 3.5.4 Comparative Analysis of Magnetic Field Data Across Multiple Survey Passes

In this segment of my analysis, I focus on demonstrating the reproducibility and reliability of magnetic field measurements by comparing data collected during two separate passes along the same survey route. This part of the study is crucial for validating the magnetic field data correction techniques and understanding the consistency of magnetic anomalies detected over time.

The visualization is carried out using scatter plots overlaid on a base map provided by OpenStreetMap. Each plot represents a survey pass, with points color-coded according to the normalized  $\Delta F$  values. This method visually emphasizes

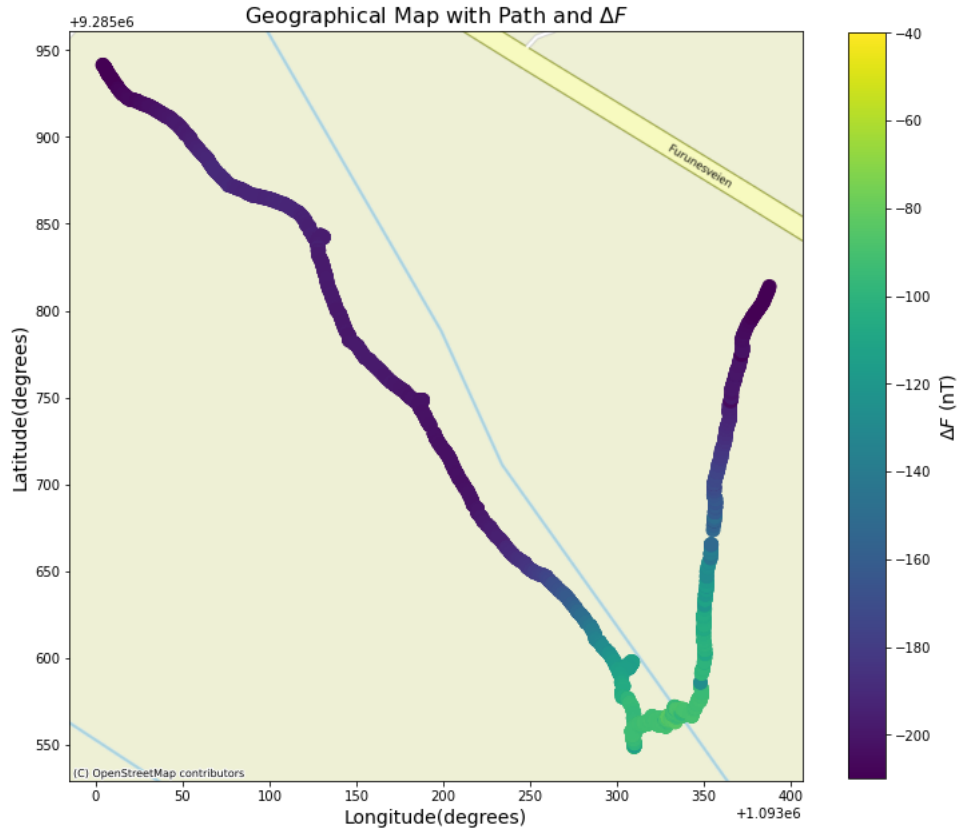


**Figure 3.5.17:** This figure displays the  $\Delta F$  measured in nanoteslas (nT) along a survey path during a specific interval (Dataset3). The color gradient from green to purple represents  $\Delta F$  ranging from -40 nT to -200 nT.

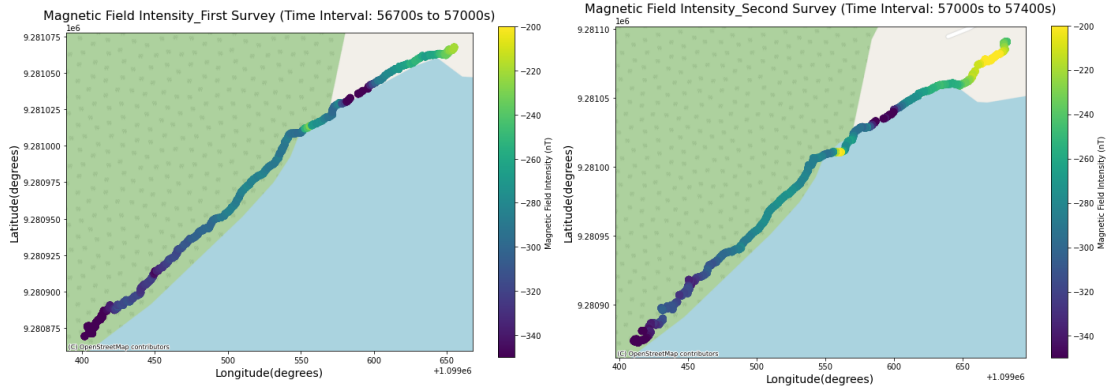


**Figure 3.5.18:**  $\Delta F$  during the First Survey **Figure 3.5.19:**  $\Delta F$  during the Second Survey (56700s to 57000s) (57000s to 57400s)

**Figure 3.5.20:** Comparative Visualization of  $\Delta F$  during Two Survey Passes. These maps showcase the magnetic field measurements taken during consecutive surveys along the same route, illustrated side by side to highlight the reproducibility of data and detect any significant variations or anomalies. The consistent color scheme across both maps allows for a direct comparison, enhancing the evaluation of temporal stability and geological influences on the magnetic field.

the geographic distribution of  $\Delta F$  and allows for direct comparison between the two surveys.

A color bar is added to each plot, serving as a legend for interpreting the  $\Delta F$  based on color. This aids in understanding the magnitude of the magnetic anomalies detected during each pass.

By analyzing the magnetic field data from two separate passes over the same route, I was able to assess the consistency of the measurements and the reliability of the data collection techniques. Similar patterns in  $\Delta F$  across the two surveys would indicate good reproducibility and suggest that any observed magnetic anomalies are not artifacts of the measurement process but likely reflect true geological features. Conversely, significant discrepancies could indicate issues with data collection consistency or environmental changes affecting the magnetic field.

This comparative analysis is essential for confirming the validity of the magnetic field data collected during the survey, providing a robust foundation for further interpretations and conclusions regarding the geological characteristics of the surveyed area.

### 3.5.5 Correlation of Magnetic Field Anomalies with Geological Features

When analyzing  $\Delta F$  diagrams in fault lines, we may encounter three models of changes in magnetic field intensity: a step change in the diagram, a peak at the fault location, or a trough. The identified magnetic anomalies in fault zones were linked to processes such as thermochemical reactions, fluid migration, and mechanical reorganization within the faults.[10]

A step change in the diagram is often due to the presence of different lithologies on either side of the fault. Different lithologies have distinct magnetic properties due to variations in mineral composition, grain size, and the presence of magnetic minerals. In the figure 3.5.21, we observe a step change in  $\Delta F$  versus longitude, which is clearly due to the lithological differences on both sides of the fault. The geological map also confirms these differences.

The provided composite image from dataset1 includes a geological map (left), a magnetic field intensity map (right), and a plot of the smoothed corrected magnetic field versus longitude (bottom)3.5.21. These visuals collectively offer insights into the geological and magnetic characteristics of the study area, specifically across a known fault line.

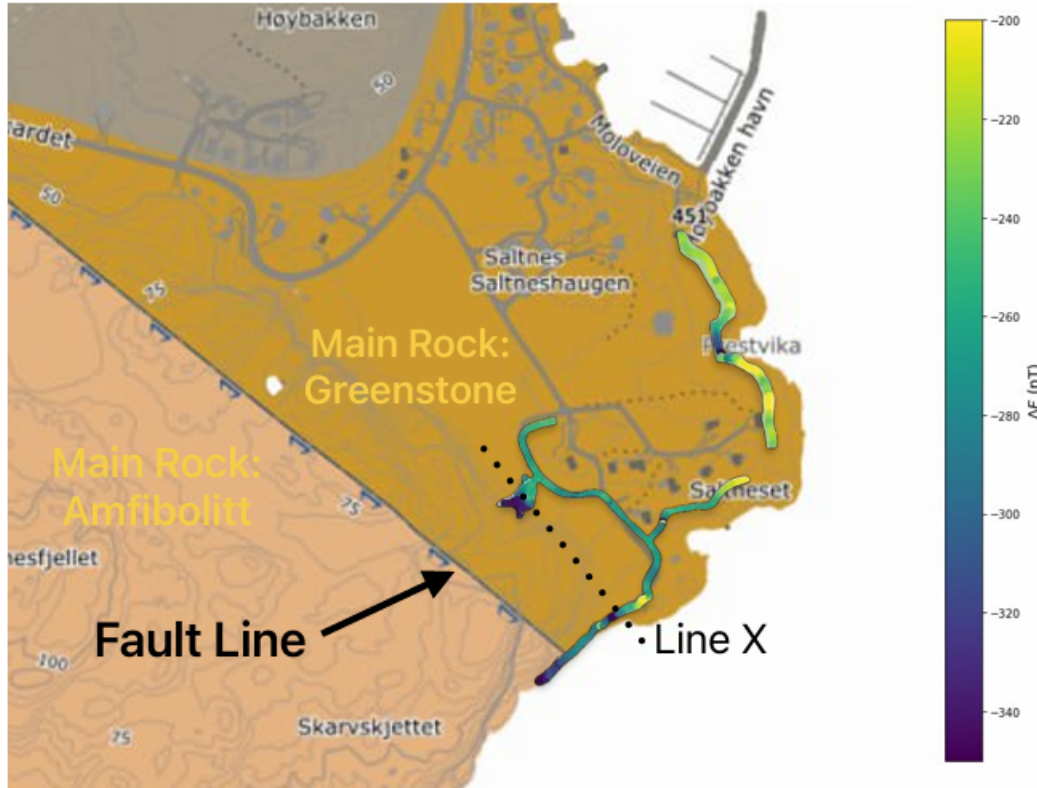
The geological map delineates the different lithologies present in the study area. The region is divided into distinct geological units, with a fault line demarcating a clear boundary between two different rock types. These lithological units exhibit varying magnetic susceptibilities, which contribute to the observed changes in the magnetic field.

The  $\Delta F$  map presents the spatial distribution of magnetic field strength along the survey path. The fault line is clearly marked, and the map shows a noticeable contrast in  $\Delta F$  on either side of the fault. This contrast is indicative of the differing magnetic properties of the lithologies present on each side of the fault.

The plot of the smoothed corrected magnetic field versus longitude further quantifies the observed changes in the  $\Delta F$  across the fault. A prominent step change is observed in the  $\Delta F$  at a specific longitude, corresponding to the location of the fault line.

The geological map confirms the presence of different lithologies on either side

### Geological Map and Magnetic Field Anomalies Across Fault Line - Dataset1



The left panel displays the geological map of the study area, highlighting different lithological units and the location of the Høybakken detachment zone. The right panel shows the magnetic field deviations map along the survey path, with the fault line clearly marked. The bottom panel presents a plot of corrected magnetic field versus longitude, illustrating a distinct change in magnetic field deviation at the fault line.

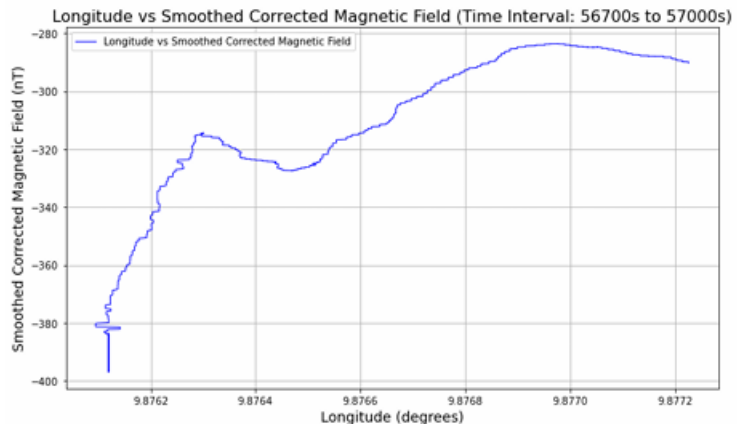


**Figure 3.5.21:** Integrated Geological and  $\Delta F$  across a Fault Line.Dataset1. Geological Map From NGU.[14]

of the fault. These lithologies are likely to have inherently different magnetic mineral compositions and concentrations, resulting in contrasting magnetic susceptibilities. The juxtaposition of these distinct rock types along the fault line explains the observed  $\Delta F$  change.

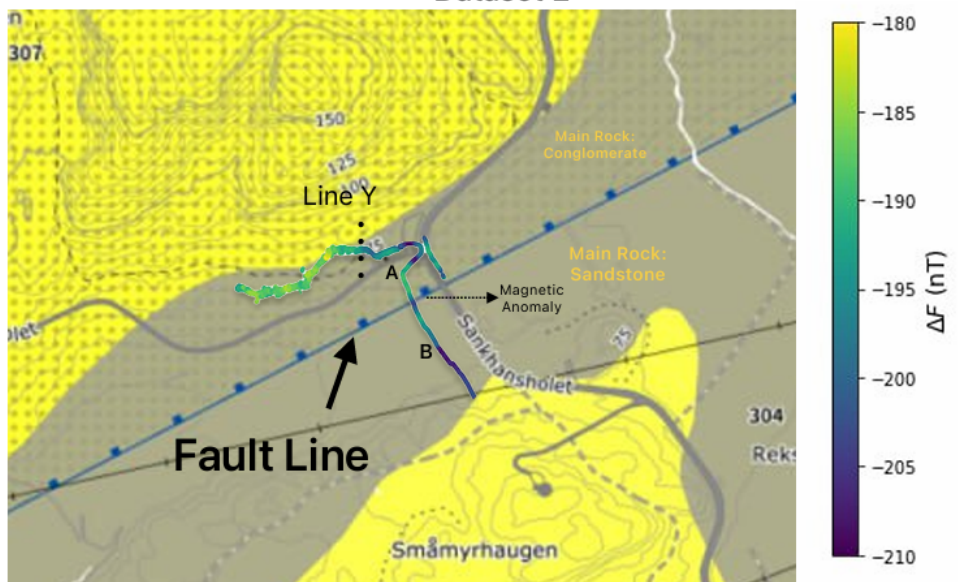
While the primary cause of the magnetic field step change is the lithological difference, faulting processes such as frictional heating, chemical alteration, and fluid percolation may also contribute to the magnetic signature. However, in this instance, the dominant factor appears to be the lithological contrast.

Line X in the map indicates two points with noticeable changes in  $\Delta F$  that

are aligned in a straight line. These two points can be related to each other. Since there is no observable fault in this geological map, these changes can be due to different lithology and rock units or because of topographical variations. The magnetic anomalies along Line X suggest variations in magnetic properties that are likely influenced by the underlying geological features or surface topography, rather than faulting.

In the figure 3.5.22, which is from dataset 2, a trough is observed in the diagram at the fault line location. The  $\Delta F$  diagram versus latitude has been plotted for the distance from point A to point B. As shown in the  $\Delta F$  spectrum on the map, the fault line is represented by the purple color, indicating a lower  $\Delta F$ , while on both sides of the fault, the diagram shows green, indicating a higher  $\Delta F$ . The magnetic field diagram clearly shows a significant decrease in  $\Delta F$  intensity at the fault line.

**Geological Map and Magnetic Field Anomalies Across Fault Line Dataset 2**



The top panel shows the geological map of the study area, illustrating different lithological units and the fault line (represented by the dashed line). This map is centered on the intersection of the Høybakken detachment fault with the Møre-Trøndelag Fault Complex. The magnetic field anomaly map overlay reveals variations in magnetic field deviations strength along the survey path. The bottom panel displays the plot of magnet field deviation versus latitude, highlighting significant fluctuations in magnetic field anomaly as the survey crosses the fault zone.

**Figure 3.5.22:** Integrated Geological and  $\Delta F$  Data across a Fault Line. Dataset 2. Geological Map From NGU.[14]

The factors contributing to this decrease are related to faulting processes. One reason could be the change in the size and alignment of magnetic particles caused by the high stress and friction during the faulting process. Finer particles typically have lower magnetic susceptibility. Another reason could be the chemical

alteration and dissolution of minerals, which change the magnetic properties of the fault zone minerals, resulting in a lower  $\Delta F$  in that area. The thermal energy released during faulting can cause localized melting in the fault zone, forming pseudotachylytes. The subsequent cooling and crystallization of these melts can imprint a new thermoremanent magnetization (TRM). However, if the frictional heating is intense enough, it can also lead to the decomposition of preexisting magnetic minerals, reducing their concentration and thus the  $\Delta F$ . This thermal alteration often results in a distinct drop in magnetic susceptibility within the fault zone.

Line Y in the picture shows a noticeable change in  $\Delta F$ , which is not associated with any fault. However, the geological map indicates a different lithology around Line Y. This difference in lithology is clearly reflected in the  $\Delta F$  spectrum, highlighting the contrasting magnetic properties of the rock units in this area. The observed magnetic anomalies along Line Y are likely due to these lithological differences rather than the presence of a fault, demonstrating how variations in rock types can significantly influence magnetic field measurements.

In figure 3.5.23, we observe an increase and peak in the  $\Delta F$  versus longitude, which is clearly visible in the  $\Delta F$  spectrum overlay on the geological map along the survey path. At the fault location, the  $\Delta F$  spectrum shifts to yellow, indicating an increase in the  $\Delta F$  of the rocks within the fault zone. Given that the lithology remains consistent along the entire survey path (as confirmed by the geological map), this change in  $\Delta F$  is certainly due to faulting processes within the fault zone.

This increase can be attributed to thermochemical reactions. Frictional heating caused by the faulting process can lead to the formation of magnetic minerals such as hematite or magnetite through thermochemical reactions. These minerals can account for the increased magnetic field intensity within the fault zone.

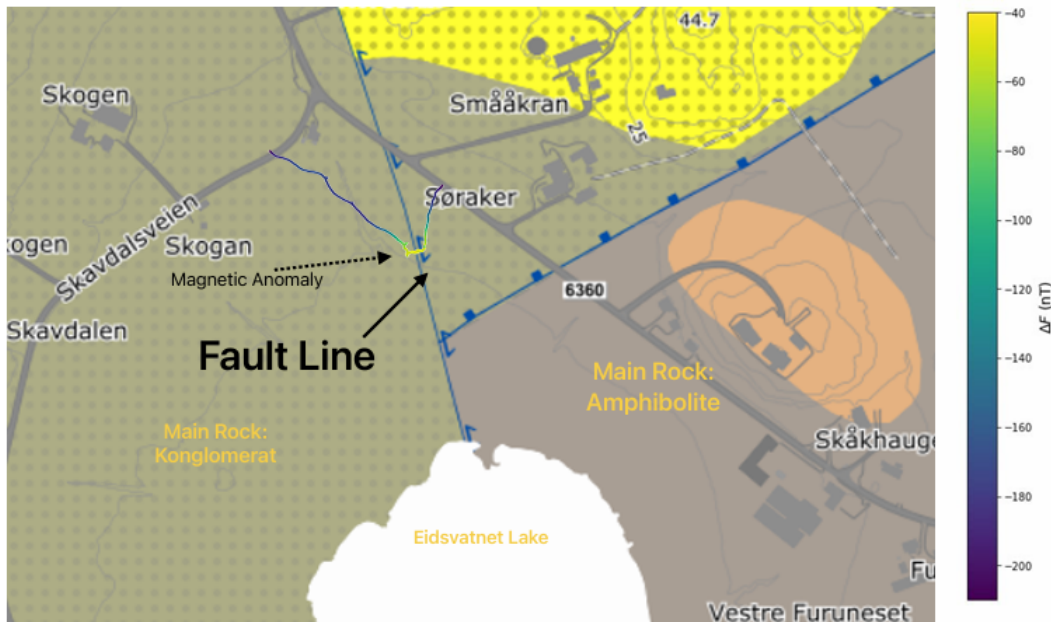
Another factor that could contribute to this peak in magnetic field intensity is post-seismic fluid migration. This process can result in the concentration and precipitation of ferrimagnetic minerals within the fault zone. As fluids percolate through the fault, they can transport and deposit iron-bearing minerals, thereby increasing the local concentration of magnetic minerals.

Mechanical effects during fault formation also play a significant role in increasing the magnetic field intensity within the fault zone. The intense shearing and deformation in a fault zone can reorient magnetic minerals and align them in such a way that enhances their collective magnetic signal. This mechanical reorganization can lead to an increase in remanent magnetization, producing a peak in  $\Delta F$  diagram.

Large earthquakes can generate significant electric currents along fault lines, known as earthquake lightning. These electric currents can induce strong isothermal remanent magnetization (IRM) in fault rocks, leading to an increase in magnetic field intensity. This phenomenon is particularly relevant in areas with a high concentration of conductive minerals.

Given the geology of the area as shown in the geological map, the main rocks in this region are sandstone and claystone, which can contain iron-bearing minerals. These minerals can transition into magnetic phases under the influence of frictional heating. Additionally, the porosity and permeability of sandstone and claystone provide a good potential for fluid pathways. This process facilitates the

### Geological Map and Magnetic Field Anomalies Across Fault Line Dataset3



The top panel displays the geological map of the study area, indicating different lithological units and the location of the fault line (marked with a dashed line). This map is focused on the transition zone between the footwall and hanging wall of the Høybakken detachment fault. The magnetic field anomalies map overlay shows variations in magnetic field strength along the survey path, with significant changes observed near the fault. The bottom panel present a plot of the magnetic field deviations versus longitude, illustrating a peak in magnetic field deviations at the fault line.

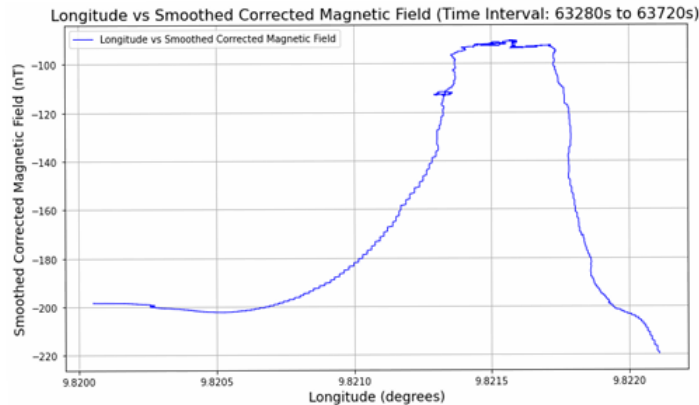


**Figure 3.5.23:** Integrated Geological and  $\Delta F$  Data across a Fault Line.Dataset3. Geological Map From NGU.[14]

transport and infiltration of iron-bearing minerals into the fault zone, increasing the magnetic field intensity.

### 3.5.6 Summary of Methodology

The methodology employed in this research focuses on collecting and analyzing magnetic field data to identify geological faults and understand their impact on magnetic field diagrams. The key steps in the methodology are as follows:

- **Survey Design and Equipment**
  - **Survey Area and Transects:** The survey was conducted in the Høybakken detachment zone, specifically focusing on the Ottersbo fault. Transects were strategically placed to minimize magnetic interference

from external sources such as residential houses and power cables. The placement also considered safety and accessibility.

- **Magnetometers:** Two types of magnetometers were used: a base magnetometer and a wearable G-859AP magnetometer. The base magnetometer was positioned at a fixed location to continuously record the base magnetic field, providing a reference for the survey. The G-859AP wearable magnetometer was used for mobile surveys along the transects, capturing magnetic field data at high resolution.

- **Data Collection**

- **Magnetic Field Measurements:** The base magnetometer recorded the magnetic field at a rate of 6 readings per minute, ensuring continuous monitoring of the base field. The wearable magnetometer recorded data at 5 readings per second during the transect surveys. Both devices were equipped with non-volatile memory for data storage.
- **Georeferencing:** The G-859AP magnetometer was integrated with a GPS system to record positional data simultaneously with magnetic measurements. This setup ensured accurate mapping of magnetic field variations along the survey paths.

- **Data Calibration and Quality Control**

- **Calibration:** Before data collection, both magnetometers were calibrated to ensure measurement accuracy. This involved adjusting zero field offsets and validating sensor orientations.
- **Quality Control:** During data collection, validation procedures were implemented to ensure data quality. This included periodic checks for sensor stability and functionality, as well as real-time identification of anomalies. Detailed field notes were taken to document environmental conditions and any deviations from the planned methodology.

- **Data Processing**

- **Data Import and Synchronization:** Magnetic field and GPS data were imported from Excel files. Since the data from the base and wearable magnetometers were collected at different intervals, synchronization was necessary. Interpolation was used to align the time stamps of the magnetic field data with the base data for accurate comparison.
- **Outlier Removal and Correction:** Outliers in the magnetic field data were identified and removed to refine data quality. The International Geomagnetic Reference Field (IGRF) model was applied to correct the raw magnetic data, isolating local anomalies by subtracting the global geomagnetic field influence.
- **Smoothing and Visualization:** Smoothing techniques were applied to reduce noise and highlight significant trends in the data. The processed data was then visualized over time to identify patterns or anomalies that could be linked to geological structures.

- **Geospatial Visualization**

- **Mapping Magnetic Field Intensity:** Cleaned and interpolated magnetic field data, along with GPS coordinates, were structured into a geospatial data frame. This allowed for accurate mapping of magnetic field variations over geographic locations using standard coordinate reference systems and geographic projections.
- **Comparative Analysis:** The magnetic field data from multiple survey passes were compared to assess reproducibility and reliability. Visualizations, including 2D and 3D plots, were created to depict the spatial distribution of  $\Delta F$  and to highlight significant anomalies.

This comprehensive methodology ensured the collection of high-quality magnetic field data, allowing for detailed analysis of magnetic anomalies and their correlation with geological faults. The findings from this research provide valuable insights into the use of geomagnetic methods for fault identification and the understanding of fault-induced magnetic variations.

### 3.5.7 Relevance to Research Objectives

The results and interpretations derived from the collected magnetic field data are integral to achieving the research objectives and addressing the hypotheses posed at the outset of this study.

#### 3.5.7.1 Identification of Faults Using Geomagnetic Methods

The primary objective of this research was to determine the effectiveness of geomagnetic methods for identifying geological faults. The processed magnetic field data revealed significant anomalies correlated with known fault locations. These anomalies, characterized by step changes, peaks, and troughs in  $\Delta F$  diagrams, confirm that geomagnetic methods can reliably detect faults. This supports Hypothesis 1, which posits a significant correlation between magnetic anomalies and fault locations.

#### 3.5.7.2 Impact of Faults on $\Delta F$ Diagrams

The study also aimed to understand how faults influence  $\Delta F$  diagrams. The data showed distinct patterns of magnetic field variations at fault zones, with observable changes such as step-like transitions and localized peaks or troughs. These patterns indicate that faults significantly alter the magnetic field, providing visual and quantitative evidence of fault presence and behavior. This finding aligns with Hypothesis 2, suggesting that faults create detectable magnetic field anomalies that can be mapped and analyzed.

#### 3.5.7.3 Reasons for Magnetic Anomalies in Fault Zones

Understanding the underlying reasons for magnetic anomalies observed in fault zones was another critical objective. The interpretation of the magnetic data, in conjunction with the geological context of the study area (sandstone and claystone

lithologies), suggests that the anomalies are caused by specific faulting processes. These include:

- **Thermochemical Reactions:** Frictional heating during faulting likely induced thermochemical reactions, forming magnetic minerals such as magnetite and hematite, which  $\Delta F$ .
- **Post-Seismic Fluid Migration:** The porosity and permeability of sandstone and claystone facilitated fluid migration, leading to the concentration and precipitation of ferrimagnetic minerals in the fault zone.
- **Mechanical Reorganization:** The intense shearing and deformation within the fault zone reoriented magnetic minerals, enhancing their collective magnetic signal.

These interpretations validate Hypothesis 3, which posits that specific faulting processes are responsible for the observed magnetic anomalies. The research findings demonstrate that magnetic anomalies in fault zones result from a combination of thermochemical, mechanical, and fluid-related processes.



---

CHAPTER  
**FOUR**

---

## RESULTS AND CONCLUSION

The analysis of the magnetic field data collected from the Høybakken detachment zone, yielded significant findings related to the research objectives. The processed data revealed clear magnetic anomalies associated with the fault zones. These anomalies were characterized by distinct step changes, peaks, and troughs in the  $\Delta F$  diagrams.

The step changes in the  $\Delta F$  diagram, observed across the fault lines, were consistent with the presence of different lithologies on either side of the faults. These lithological differences, primarily between sandstone and claystone, contributed to variations in magnetic properties due to their distinct mineral compositions and grain sizes. This finding confirms that geomagnetic methods can effectively identify faults by detecting abrupt changes in  $\Delta F$ .

Additionally, the presence of peaks and troughs in the  $\Delta F$  diagrams indicated localized increases and decreases in magnetic field anomalies at the fault locations. These variations were attributed to faulting processes such as thermochemical reactions, post-seismic fluid migration, and mechanical reorganization of magnetic minerals. Specifically, frictional heating during faulting likely induced the formation of magnetic minerals like magnetite and hematite, which increased the  $\Delta F$ . The porosity and permeability of sandstone and claystone facilitated fluid migration, leading to the concentration and precipitation of ferrimagnetic minerals in the fault zone. Intense shearing and deformation within the fault zone reoriented magnetic minerals, enhancing their collective magnetic signal.

The results of this research demonstrate the effectiveness of geomagnetic methods in identifying geological faults. The significant correlations between magnetic anomalies and fault locations provide strong evidence that faults can be reliably detected using magnetic field data. The observed patterns in the  $\Delta F$  diagrams, including step changes, peaks, and troughs, illustrate how faults influence magnetic field anomalies.

The study also elucidates the underlying reasons for magnetic anomalies in fault zones. The identified faulting processes (thermochemical reactions, post seismic fluid migration, and mechanical reorganization) explain the variations in  $\Delta F$  observed at fault locations. These findings highlight the complex interplay between geological processes and magnetic properties, enhancing our understanding of fault zone dynamics.

In conclusion, this research advances the field of geophysics by improving fault

detection techniques and the interpretation of magnetic data in geological surveys. The integration of geomagnetic methods with detailed geological analysis provides a powerful tool for identifying and understanding geological faults. Future research should continue to explore these methodologies in different geological settings to further validate and refine these techniques.

## 4.1 Future Work Suggestions

In future research, a key focus can be on how geomagnetic methods can be used to identify fractures and faults in hydrocarbon reservoirs and monitor changes in these fractures over time. This approach could significantly enhance our ability to detect and characterize subsurface structures in hydrocarbon exploration and production, providing valuable insights into reservoir dynamics and integrity. Here are some detailed suggestions for future work in this area:

- **Development of Real-Time Monitoring Systems:** Implement real-time monitoring systems using geomagnetic sensors to continuously track changes in magnetic fields associated with fractures and faults in hydrocarbon reservoirs. This could provide early warning signs of structural changes or potential hazards, improving reservoir management and safety.
- **Integration with Reservoir Simulation Models:** Integrate geomagnetic data with reservoir simulation models to enhance the accuracy of predicting fluid flow and reservoir behavior. This combined approach can help optimize hydrocarbon production and recovery by providing a more comprehensive understanding of reservoir dynamics.
- **Long-Term Studies:** Conduct cost-benefit analyses to evaluate the economic feasibility of implementing geomagnetic monitoring systems in hydrocarbon reservoirs. This analysis can help in making informed decisions about the adoption of these technologies in the industry, balancing cost with potential benefits.

By pursuing these future research directions, the application of geomagnetic methods in the oil and gas industry can be significantly enhanced, leading to more efficient, safe, and sustainable hydrocarbon extraction processes.

## REFERENCES

- [1] Isabelle Moretti. “The role of faults in hydrocarbon migration”. In: *Petroleum Geoscience* 4 (Feb. 1998), pp. 81–94. DOI: [10.1144/petgeo.4.1.81](https://doi.org/10.1144/petgeo.4.1.81).
- [2] Jing Li et al. “Automatic Preidentification of Fault Structural Traps From Graph View”. In: *IEEE Geoscience and Remote Sensing Letters* 19 (2022), pp. 1–5. DOI: [10.1109/LGRS.2022.3184522](https://doi.org/10.1109/LGRS.2022.3184522).
- [3] *Geology In / All About Geology*. Accessed: 2024-06-04. 2024. URL: <https://www.geologyin.com/>.
- [4] S. J. Jolley, Q. J. Fisher, and R. B. Ainsworth. “Reservoir compartmentalization: an introduction”. In: *Geological Society, London, Special Publications* 347.1 (2010), pp. 1–8. DOI: [10.1144/SP347.1](https://doi.org/10.1144/SP347.1). eprint: <https://www.lyellcollection.org/doi/pdf/10.1144/SP347.1>. URL: <https://www.lyellcollection.org/doi/abs/10.1144/SP347.1>.
- [5] Unknown. “Methods of Fault Detection”. In: *Recorder* (Sept. 2019). Page 17. URL: [/mnt/data/2019-09-RECORDER-Methods\\_of\\_fault\\_detection.pdf](https://mnt/data/2019-09-RECORDER-Methods_of_fault_detection.pdf).
- [6] Jennifer Cunningham et al. “The Impact of Seismic Interpretation Methods on the Analysis of Faults: A Case Study from the Snøhvit Field, Barents Sea”. In: (Oct. 2020). DOI: [10.5194/se-2020-174](https://doi.org/10.5194/se-2020-174).
- [7] W Tanikawa Mark J Dekkers. “New insights from the magnetic properties of fault rocks”. In: (Nov. 2020). DOI: [10.1029/2020E0151611](https://doi.org/10.1029/2020E0151611).
- [8] Tao Yang et al. “Faulting Processes Unveiled by Magnetic Properties of Fault Rocks”. In: *Reviews of Geophysics* 58.4 (), e2019RG000690. DOI: <https://doi.org/10.1029/2019RG000690>. eprint: <https://agupubs.onlinelibrary.wiley.com/doi/pdf/10.1029/2019RG000690>. URL: <https://agupubs.onlinelibrary.wiley.com/doi/abs/10.1029/2019RG000690>.
- [9] Zongxuan Wu et al. “Detection and characterization of geomagnetic anomaly waveforms”. In: *Journal of Asian Earth Sciences* 259 (2024), p. 105837. ISSN: 1367-9120. DOI: <https://doi.org/10.1016/j.jseaes.2023.105837>. URL: <https://www.sciencedirect.com/science/article/pii/S1367912023002985>.
- [10] Hazeez Owolabi Edunjobi et al. “Qualitative interpretation of high resolution aeromagnetic data of abeokuta metropolis for geological characterisation”. In: *Results in Geophysical Sciences* 15 (2023), p. 100062. ISSN: 2666-8289. DOI: <https://doi.org/10.1016/j.ringps.2023.100062>. URL: <https://www.sciencedirect.com/science/article/pii/S2666828923000123>.

- [11] Chronosurveys Lda. Il Machado. *A Simple Guide to Seismic Horizon Interpretation*. Aug. 2020. URL: [geoexpro.com/a-simple-guide-to-seismic-horizon-interpretation/](http://geoexpro.com/a-simple-guide-to-seismic-horizon-interpretation/).
- [12] Per-Terje Osmundsen et al. “Kinematics of the Høybakken detachment zone and the MøreTrøndelag Fault Complex, central Norway”. In: *Journal of the Geological Society* 163 (Jan. 2006), pp. 303–318.
- [13] Christopher Leech Manor Farm Cottage Galley Lane Great Brickhill Bucks.MK17 Geometrics Europe. *G-859AP MINING MAG Cesium Magnetometer*. GEOMETRICS, INC, 2011.
- [14] Norwegian Geological Survey (NGU). *Geological Maps*. Accessed: 2024-05-30. 2024. URL: <https://www.ngu.no>.

# APPENDIXES

## .1 Python Codes

```
import pandas as pd
import matplotlib.pyplot as plt
from scipy import stats
from scipy.interpolate import interp1d
import geopandas as gpd
import contextily as ctx
from matplotlib.colors import Normalize
from matplotlib import cm
import numpy as np
from shapely.geometry import LineString
import pyIGRF
import time
from datetime import datetime
from mpl_toolkits.mplot3d import Axes3D
from shapely.geometry import Point
import pyproj
from pyproj import Transformer
from pyproj import Proj, transform
from owslib.wms import WebMapService
from matplotlib.cm import ScalarMappable

# Define Functions
def timetosecond(n):
    n = int(n)
    hr, remainder = divmod(n, 10000)
    minute, sec = divmod(remainder, 100)
    return hr * 3600 + minute * 60 + sec

def time_to_datetime(timebase):
    time_str = str(timebase).zfill(6)
    time_obj = datetime.strptime(time_str, '%H%M%S').time()
    date_obj = datetime(2023, 8, 18)
    return datetime.combine(date_obj, time_obj)

def calculate_igrf(date, latitude, longitude, altitude=0):
    if not isinstance(date, datetime):
        raise ValueError(f"Expected datetime, got {type(date)}")
    year = date.year + (date.month - 1) / 12 + (date.day - 1) /
          365.25
```

```

    igrf_result = pyIGRF.igrf_value(latitude, longitude, altitude,
                                    year)
    return igrf_result[-1]

# Load Datasets
F_path = 'C:/ntnu/thesis/Second Time/DATASET4/magnetic_field_data.
           xlsx',
Base_path = 'C:/ntnu/thesis/base data.xlsx',
GPS_path = 'C:/ntnu/thesis/Second Time/DATASET4/gps_location_data4
           .xlsx'

Base_data = pd.read_excel(Base_path)
F_data = pd.read_excel(F_path)
GPS_data = pd.read_excel(GPS_path)

Output = 'C:/ntnu/thesis/Second Time/DATASET4/Output.xlsx'
Output2 = 'C:/ntnu/thesis/Second Time/DATASET4/Output2.xlsx'

# Time Converting
F_data['Time'] = F_data['Time'].fillna(method='ffill').astype(int)

# Convert 'Time' to string and ensure it's in 'HHMMSS' format
F_data['Time'] = F_data['Time'].astype(str).str.zfill(6)

Base_data['timebase'] = Base_data['timebase'].apply(
    time_to_datetime)
F_data['datetime'] = F_data['Time'].apply(time_to_datetime)
GPS_data['datetime'] = GPS_data['Time'].apply(time_to_datetime)

#interpolating to find missing data
F_data['datetime'] = pd.to_datetime(F_data['Time'], format='%H%M%S
           ')
F_data.set_index('datetime', inplace=True)

F_data_resampled = F_data.resample('S').mean().interpolate(method=
           'linear', limit_direction='both')
F_data_resampled.to_excel(Output2)

#Interpolating Base data in magnetic field data
base_timestamps = Base_data['timebase'].apply(lambda dt: dt.
                                               timestamp())
f_timestamps = F_data['datetime'].apply(lambda dt: dt.timestamp())
Ynew = np.interp(f_timestamps, base_timestamps, Base_data['
           magneticfield'])
F_data['Interpolated_Magnetic_Field'] = Ynew

#Merge GPS data with Magnetic field Data
F_data = F_data.sort_values(by='datetime')
GPS_data = GPS_data.sort_values(by='datetime')
F_data = pd.merge_asof(F_data, GPS_data[['datetime', 'Latitude', 'Longitude']], on='datetime',
                       direction='nearest')

#Calculating IGRF
F_data['IGRF_F'] = F_data.apply(lambda row: calculate_igrf(row['
           datetime'], row['Latitude'], row['Longitude']), axis=1)
F_data['variation'] = F_data['IGRF_F'] - Ynew

```

```

# Remove outliers from Original Magnetic Field
Q1 = F_data['Magnetic_Field'].quantile(0.25)
Q3 = F_data['Magnetic_Field'].quantile(0.75)
IQR = Q3 - Q1
lower_bound = Q1 - 1.5 * IQR
upper_bound = Q3 + 1.5 * IQR
F_data = F_data[(F_data['Magnetic_Field'] >= lower_bound) & (
                    F_data['Magnetic_Field'] <=
                    upper_bound)]

#Plot Original Magnetic field in Time
Time_for_plot = np.array([timetosecond(n) for n in F_data['Time']])
plt.figure(figsize=(10, 6))
plt.plot(Time_for_plot, F_data['Magnetic_Field'], label='Magnetic Filed Over Time', color='blue',
          linewidth=1)
plt.title('Original Magnetic Field Variation Over Time', fontsize=16)
plt.xlabel('Time(Seconds)', fontsize=14)
plt.ylabel('Magnetic Field (nT)', fontsize=14)
plt.grid(True)
plt.legend()
plt.xticks(rotation=45)
plt.tight_layout()

plt.show()

#Correcting Magnetic Filed
F_data['Magnetic_Field_Corrected']=F_data['Magnetic_Field'] -
                                    F_data['IGRF_F'] - F_data['variation']

F_data['Time_for_plot'] = Time_for_plot
output_df = F_data[['Time_for_plot', 'IGRF_F', 'Interpolated_Magnetic_Field',
                    'variation', 'Magnetic_Field_Corrected']]
output_df.to_excel(Output, index=False)

F_data = F_data[(F_data['Magnetic_Field_Corrected'] > -410) & (
                    F_data['Magnetic_Field_Corrected'] < -150)]

Time_for_plot = np.array([timetosecond(n) for n in F_data['Time']])
plt.figure(figsize=(10, 6))
plt.plot(Time_for_plot, F_data['Magnetic_Field_Corrected'], label='Magnetic Field Corrected (Subtract IGRF)', color='blue',
          linewidth=1)
plt.title('Corrected Magnetic Field Over Time', fontsize=16)
plt.xlabel('Time(Seconds)', fontsize=14)

```

```

plt.ylabel('Magnetic Field (nT)', fontsize=14)
plt.grid(True)
plt.legend()
plt.xticks(rotation=45)
plt.tight_layout()

plt.show()

#Smoothing Data
window_size = 100
F_data['Magnetic_Field_Corrected_Smoothed'] = F_data['Magnetic_Field_Corrected'].rolling(window=window_size).mean()

# Plot Corrected Smoothed Magnetic Field Over Time
plt.figure(figsize=(10, 6))
plt.plot(Time_for_plot, F_data['Magnetic_Field_Corrected_Smoothed'], label='Smoothed Corrected Magnetic Field', color='blue', linewidth=1)
plt.title('Smoothed Corrected Magnetic Field Over Time', fontsize=16)
plt.xlabel('Time(Seconds)', fontsize=14)
plt.ylabel('Magnetic Field (nT)', fontsize=14)
plt.grid(True)
plt.legend()
plt.xticks(rotation=45)
plt.tight_layout()

plt.show()

# Calculate the absolute difference between each point and its predecessor
F_data['Magnetic_Field_Diff'] = F_data['Magnetic_Field_Corrected'].diff().abs()
threshold = F_data['Magnetic_Field_Diff'].std() * 3
sharp_peaks_times = F_data[F_data['Magnetic_Field_Diff'] > threshold]['datetime']
print(sharp_peaks_times)

# Correcting magnetic field data
F_data['z_score'] = stats.zscore(F_data['Magnetic_Field'])
F_data_clean = F_data[F_data['z_score'].abs() <= 3]
F_data_clean['correctionF'] = F_data_clean['Magnetic_Field'] - F_data['IGRF_F'] - F_data['variation']

print("Data type of 'Time':", F_data_clean['Time'].dtype)

if F_data_clean['Time'].dtype == 'object':
    F_data_clean['Time'] = pd.to_numeric(F_data_clean['Time'], errors='coerce')

```

```

    print("Number of NaNs after conversion:", F_data_clean['Time']
          .isna().sum())

F_data_clean['Time'] = F_data_clean['Time'].astype(float)

F_data['Time_in_seconds'] = [timetosecond(time) for time in F_data
                             ['Time']]

# Load the GPS dataset
GPS_data = pd.read_excel(GPS_path)

def remove_outliers(df, columns):
    for column_name in columns:
        Q1 = df[column_name].quantile(0.25)
        Q3 = df[column_name].quantile(0.75)
        IQR = Q3 - Q1
        lower_bound = Q1 - 1.5 * IQR
        upper_bound = Q3 + 1.5 * IQR
        df = df[(df[column_name] >= lower_bound) & (df[column_name]
                                                       ] <= upper_bound)]
    return df

# Removing outliers
columns_to_clean = ['Latitude', 'Longitude', 'Altitude']

GPS_data_cleaned = remove_outliers(GPS_data, columns_to_clean)

longitude_data = GPS_data_cleaned['Longitude']
latitude_data = GPS_data_cleaned['Latitude']
altitude_data = GPS_data_cleaned['Altitude']

# Convert time for plotting
GPS_time=np.array([timetosecond(n) for n in GPS_data_cleaned['Time']
                  ]])

plt.figure(figsize=(15, 15))

# Plotting Latitude
plt.subplot(3, 1, 1)
plt.plot(GPS_time, GPS_data_cleaned['Latitude'], label='Latitude',
          color='blue')
plt.xlabel('Time(seconds)', fontsize=14)
plt.ylabel('Latitude(degrees)', fontsize=14)
plt.title('Latitude Variation Over Time', fontsize=16)
plt.legend()
plt.grid(True)

# Plotting Longitude
plt.subplot(3, 1, 2)
plt.plot(GPS_time, GPS_data_cleaned['Longitude'], label='Longitude',
          color='green')
plt.xlabel('Time(seconds)', fontsize=14)
plt.ylabel('Longitude(degrees)', fontsize=14)
plt.title('Longitude Variation Over Time', fontsize=16)
plt.legend()
plt.grid(True)

```

```

# Plotting Altitude
plt.subplot(3, 1, 3)
plt.plot(GPS_time, GPS_data_cleaned['Altitude'], label='Altitude',
         color='red')
plt.xlabel('Time(seconds)', fontsize=14)
plt.ylabel('Altitude(meters)', fontsize=14)
plt.title('Altitude Variation Over Time', fontsize=16)
plt.legend()
plt.grid(True)

plt.tight_layout()
plt.show()

interp_latitude = interp1d(GPS_data_cleaned['Time'],
                           GPS_data_cleaned['Latitude'],
                           kind='linear', fill_value="extrapolate")
interp_longitude = interp1d(GPS_data_cleaned['Time'],
                             GPS_data_cleaned['Longitude'],
                             kind='linear', fill_value="extrapolate")
interp_Altitude = interp1d(GPS_data_cleaned['Time'],
                           GPS_data_cleaned['Altitude'],
                           kind='linear', fill_value="extrapolate")

# Apply the interpolation to create the new columns on the
# DataFrame that has the 'Time' column
# This should be the DataFrame with magnetic field data sampled
# every 0.2 seconds.
F_data_clean['Interp_Latitude'] = interp_latitude(F_data_clean['Time'])
F_data_clean['Interp_Longitude'] = interp_longitude(F_data_clean['Time'])
F_data_clean['Interp_Altitude'] = interp_Altitude(F_data_clean['Time'])

# 3D plot
fig = plt.figure(figsize=(10, 7))
ax = fig.add_subplot(111, projection='3d')

sc = ax.scatter(F_data_clean['Interp_Latitude'], F_data_clean['Interp_Longitude'],
                 F_data_clean['Interp_Altitude'], c=F_data_clean['correctionF'], cmap='viridis')

ax.set_xlabel('Latitude(degrees)', fontsize=14)
ax.set_ylabel('Longitude(degrees)', fontsize=14)
ax.set_zlabel('Altitude(meters)', fontsize=14)

cbar = fig.colorbar(sc, ax=ax, shrink=0.5, aspect=5)
cbar.set_label('Corrected Magnetic Field (nT)', fontsize=14)

plt.title('3D Plot of Corrected Magnetic Field Variation Over GPS
Coordinates', fontsize=16)

```

```

plt.show()

#2D plot
plt.figure(figsize=(12, 6))

scatter = plt.scatter(F_data_clean['Interp_Longitude'],
                      F_data_clean['Interp_Latitude'],
                      c=F_data_clean['correctionF'],
                      cmap='viridis')

cbar = plt.colorbar(scatter)
cbar.set_label('Magnetic Field Intensity(nT)', fontsize=14)

plt.xlabel('Longitude(degrees)', fontsize=14)
plt.ylabel('Latitude(degrees)', fontsize=14)
plt.title('Interpolated Magnetic Field Intensity Map', fontsize=16
          )

plt.legend()

plt.show()

# Plot data on geographical map
gdf = gpd.GeoDataFrame(
    F_data_clean,
    geometry=gpd.points_from_xy(F_data_clean['Interp_Longitude'],
                                 F_data_clean['Interp_Latitude']
                                 ])
)

gdf.crs = "EPSG:4326"

gdf = gdf.to_crs(epsg=3857)

min_magnetic_field = -350
max_magnetic_field = -200

norm = Normalize(vmin=min_magnetic_field, vmax=max_magnetic_field)

cmap = cm.viridis

fig, ax = plt.subplots(figsize=(10, 10))

scatter = ax.scatter(gdf.geometry.x, gdf.geometry.y, c=gdf['
                           correctionF'], cmap='viridis',
                           norm=Normalize(vmin=-350, vmax=-
                           200), s=100) # Fixed size for
                           visibility

try:
    ctx.add_basemap(ax, crs=gdf.crs.to_string(), source=ctx.
                    providers.OpenStreetMap.
                    Mapnik, zoom="auto")
except Exception as e:
    print("Failed to load base map:", e)

```

```

ax.set_aspect('equal')
plt.tight_layout()

cbar = fig.colorbar(ScalarMappable(norm=Normalize(vmin=-350, vmax=-200), cmap='viridis'), ax=ax, orientation='vertical', shrink=1)
cbar.set_label('Magnetic Field Intensity (nT)', fontsize=14)

plt.title('Geographical Map with Path and Magnetic Field Intensity', fontsize=16)
plt.xlabel('Longitude(degrees)', fontsize=14)
plt.ylabel('Latitude(degrees)', fontsize=14)
plt.show()

# Export the DataFrame to an Excel file
all_data = pd.DataFrame({
    'Time': F_data_clean['Time'],
    'Time_in_Seconds': F_data['Time_in_seconds'],
    'Original Magnetic Field': F_data['Magnetic_Field'],
    'IGRF Magnetic Field': F_data['IGRF_F'],
    'Magnetic Field Variation': F_data['variation'],
    'Z-Score': F_data['z_score'],
    'Corrected Magnetic Field': F_data_clean['correctionF'],
    'Interpolated Latitude': F_data_clean['Interp_Latitude'],
    'Interpolated Longitude': F_data_clean['Interp_Longitude'],
    'Interpolated Altitude': F_data_clean['Interp_Altitude'] #
                                            Include this only if you have
                                            altitude data
})
all_data.to_excel('combined_data.xlsx', index=False)

#comparative plots
GPS_data['Time_in_seconds'] = GPS_data['Time'].apply(timetosecond)

filtered_GPS_data1 = GPS_data[(GPS_data['Time_in_seconds'] >= 56700) & (GPS_data['Time_in_seconds'] <= 57000)]

merged_data1 = pd.merge(filtered_GPS_data1, F_data_clean, on='Time', how='inner')
print("Columns in merged_data1:", merged_data1.columns)

gdf = gpd.GeoDataFrame(
    merged_data1,
    geometry=gpd.points_from_xy(merged_data1.Longitude_x, merged_data1.Latitude_x)
)
gdf.set_crs(epsg=4326, inplace=True)
gdf = gdf.to_crs(epsg=3857)

norm = Normalize(vmin=merged_data1['Magnetic_Field_Corrected'].min(), vmax=merged_data1['Magnetic_Field_Corrected'].max())
cmap = cm.viridis # You can change the colormap to something else if you prefer

fig, ax = plt.subplots(figsize=(10, 10))

```

```

scatter = ax.scatter(gdf.geometry.x, gdf.geometry.y, c=gdf['
    correctionF'], cmap='viridis',
    norm=Normalize(vmin=-350, vmax=-200), s=100) # Fixed size for
    visibility

try:
    ctx.add_basemap(ax, crs=gdf.crs.to_string(), source=ctx.
        providers.OpenStreetMap.
        Mapnik, zoom="auto")
except Exception as e:
    print("Failed to load base map:", e)

ax.set_aspect('equal')
plt.tight_layout()

cbar = fig.colorbar(ScalarMappable(norm=Normalize(vmin=-350, vmax=-200), cmap='viridis'), ax=ax,
    orientation='vertical', shrink=0.
    6)
cbar.set_label('Magnetic Field Intensity (nT)', fontsize=14)

plt.title('Magnetic Field Intensity_First Survey (Time Interval:
    56700s to 57000s)', fontsize=16)
plt.xlabel('Longitude(degrees)', fontsize=14)
plt.ylabel('Latitude(degrees)', fontsize=14)
plt.show()

filtered_GPS_data2= GPS_data[(GPS_data['Time_in_seconds'] >= 57000
    ) & (GPS_data['Time_in_seconds'] <= 57400)]
# Merge GPS data with Magnetic field data on time
merged_data2 = pd.merge(filtered_GPS_data2, F_data_clean, on='Time
    ', how='inner')

gdf = gpd.GeoDataFrame(
    merged_data2,
    geometry=gpd.points_from_xy(merged_data2.Longitude_x,
        merged_data2.Latitude_x)
)
gdf.set_crs(epsg=4326, inplace=True)
gdf = gdf.to_crs(epsg=3857)

norm = Normalize(vmin=merged_data2['Magnetic_Field_Corrected'].min
    (), vmax=merged_data2['
        Magnetic_Field_Corrected'].max())
cmap = cm.viridis # You can change the colormap to something else
    if you prefer

fig, ax = plt.subplots(figsize=(10, 10))

scatter = ax.scatter(gdf.geometry.x, gdf.geometry.y, c=gdf['
    correctionF'], cmap='viridis',
    norm=Normalize(vmin=-350, vmax=-200), s=100) # Fixed size for
    visibility

```

```

try:
    ctx.add_basemap(ax, crs=gdf.crs.to_string(), source=ctx.
                     providers.OpenStreetMap.
                     Mapnik, zoom="auto")
except Exception as e:
    print("Failed to load base map:", e)

ax.set_aspect('equal')
plt.tight_layout()

cbar = fig.colorbar(ScalarMappable(norm=Normalize(vmin=-350, vmax=
                                                 -200), cmap='viridis'), ax=ax,
                     orientation='vertical', shrink=0.
                     6)
cbar.set_label('Magnetic Field Intensity (nT)', fontsize=14)

plt.title('Magnetic Field Intensity_Second Survey (Time Interval:
           57000s to 57400s)', fontsize=16)
plt.xlabel('Longitude(degrees)', fontsize=14)
plt.ylabel('Latitude(degrees)', fontsize=14)
plt.show()

```